

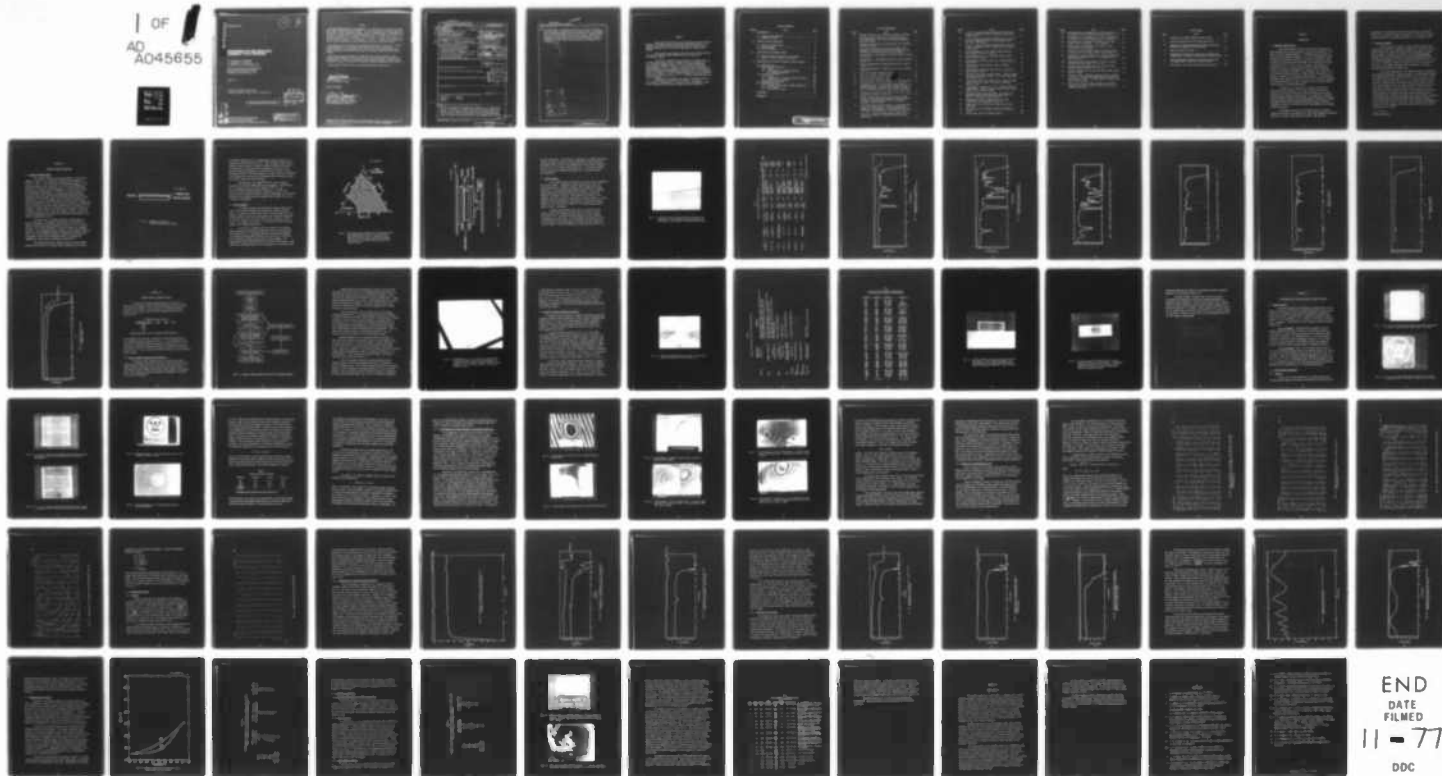
AD-A045 655

WESTINGHOUSE RESEARCH AND DEVELOPMENT CENTER PITTSBU--ETC F/G 17/5
DEVELOPMENT OF MULTISPECTRAL SANDWICH-TYPE IR WINDOWS.(U)

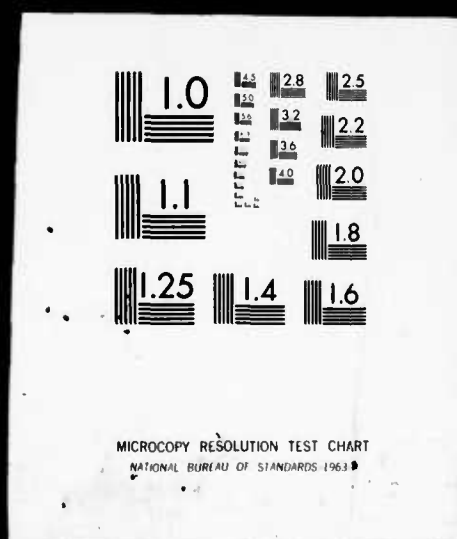
UNCLASSIFIED

APR 77 W E KRAMER, R H HOPKINS, G B BRANDT F33615-76-C-5085
77-9C4-WINDO-R1 AFML-TR-77-53 NL

1 OF
AD
A045655



1 OF 1
AD
A045655



AD A 045655

AFML-TR-77-53

12

J

DEVELOPMENT OF MULTISPECTRAL SANDWICH-TYPE IR WINDOWS

W. E. KRAMER, R. H. HOPKINS,
G. B. BRANDT, R. A. HOFFMAN,
J. SCHRUBEN, AND K. B. STEINBRUEGGE

WESTINGHOUSE ELECTRIC CORPORATION
RESEARCH & DEVELOPMENT CENTER
PITTSBURGH, PENNSYLVANIA 15235

APRIL 1977

TECHNICAL REPORT AFML-TR-77-53
Final Report for Period 1 February 1976 to 31 January 1977

Approved for Release; Distribution Unlimited.

DDC
RECEIVED
OCT 25 1977
B

AD No. _____
DDC FILE COPY

AIR FORCE MATERIALS LABORATORY
AIR FORCE SYSTEMS COMMAND
WRIGHT-PATTERSON AIR FORCE BASE, OHIO 45433

DISTRIBUTION STATEMENT A

Approved for public release;
Distribution Unlimited

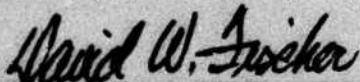
NOTICE

When Government drawings, specifications, or other data are used for any purpose other than in connection with a definitely related Government procurement operation, the United States Government thereby incurs no responsibility nor any obligation whatsoever; and the fact that the government may have formulated, furnished, or in any way supplied the said drawings, specifications, or other data, is not to be regarded by implication or otherwise as in any manner licensing the holder or any other person or corporation, or conveying any rights or permission to manufacture, use, or sell any patented invention that may in any way be related thereto.

This final report was submitted by the Westinghouse Electric Corporation, Research and Development Center, Pittsburgh, Pennsylvania 15235 under Contract No. F33615-76-C-5085, job order number 7371, with the Air Force Materials Laboratory, Wright-Patterson Air Force Base, Ohio 45433. Mr. David W. Fischer was the Project Monitor.

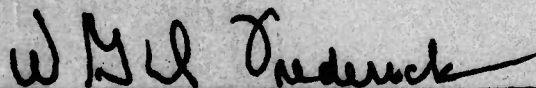
This report has been reviewed and cleared for open publication and/or public release by the appropriate Office of Information (OI) in accordance with AFR 190-17 and DOD D5230.9. There is no objection to unlimited distribution of this report to the public at large, or by DDG to the National Technical Information Service (NTIS).

This technical report has been reviewed and approved for publication.



David W. Fischer
Project Engineer/Scientist

FOR THE COMMANDER



William G. D. Frederick, Chief
Laser & Optical Materials Branch
Electromagnetic Materials Division
Air Force Materials Laboratory

Copies of this report should not be returned unless return is required by security considerations, contractual obligations, or notice on a specific document.

UNCLASSIFIED

SECURITY CLASSIFICATION OF THIS PAGE (When Data Entered)

19 REPORT DOCUMENTATION PAGE		READ INSTRUCTIONS BEFORE COMPLETING FORM	
1. REPORT NUMBER AFML TR-77-53	2. GOVT ACCESSION NO. 680500	3. RECIPIENT'S CATALOG NUMBER	
4. TITLE (and Subtitle) DEVELOPMENT OF MULTISPECTRAL SANDWICH-TYPE IR WINDOWS.		5. TYPE OF REPORT & PERIOD COVERED Final Report. 1 FEB 1976 - 31 JAN 1977.	
7. AUTHOR(s) W.E. Kramer, R.H. Hopkins, G.B. Brandt, R.A. Hoffman J. Schruben and K.B. Steinbruegge		6. PERFORMING ORG. REPORT NUMBER 77-9C4-WINDO-R1	
9. PERFORMING ORGANIZATION NAME AND ADDRESS Westinghouse Electric Corporation Research & Development Center 1310 Beulah Road, Pittsburgh, PA 15235		8. CONTRACT OR GRANT NUMBER(s) F33615-76-C-5085	
11. CONTROLLING OFFICE NAME AND ADDRESS Air Force Materials Laboratory (AFML/LPO) Air Force Systems Command Wright-Patterson AFB, Ohio 45433		10. PROGRAM ELEMENT, PROJECT, TASK AREA & WORK UNIT NUMBERS Project 7371 Task 737101 Work Unit 73710154	
14. MONITORING AGENCY NAME & ADDRESS (if different from Controlling Office)		12. REPORT DATE Apr 1977	
		13. NUMBER OF PAGES 72	
		15. SECURITY CLASS. (of this report) UNCLASSIFIED	
16. DISTRIBUTION STATEMENT (of this Report) Approved for public release; distribution unlimited.		15a. DECLASSIFICATION DOWNGRADING SCHEDULE	
17. DISTRIBUTION STATEMENT (of the abstract entered in Block 20, if different from Report)			
18. SUPPLEMENTARY NOTES 62102 F			
19. KEY WORDS (Continue on reverse side if necessary and identify by block number) multispectral sandwich window infrared composite			
20. ABSTRACT (Continue on reverse side if necessary and identify by block number) Composite or sandwich-type multispectral windows up to 4 x 6 inch in size have been fabricated by a Westinghouse-developed technique called optical brazing. Of the numerous cladding, substrate and adhesives tested, the ZnS/ZnSe composite window is now the most promising for airborne common aperture systems. Optical path differences in the assembled windows stem mainly from material property variations in the component parts, not from (over)			

UNCLASSIFIED

MICROMETER

SECURITY CLASSIFICATION OF THIS PAGE(When Data Entered)

20. the binding agent. These path differences can for the most part be corrected during final polishing of the composite window. The ZnS/ZnSe window transmittance with AR coating exceeds the 60% visible wavelength and 1.06 and 95% 8-12 μ m transmittance requirements. Composite window specimens are as rain erosion resistant as monolithic ZnS. Optical brazing is a versatile technique for composite window fabrication and has been used to join other cladding and substrate combinations such as $MgF_2/ZnSe$.

ACCESSION for	
NTIS	White Section <input checked="" type="checkbox"/>
DDC	Red Section <input type="checkbox"/>
UNCLASSIFIED	<input type="checkbox"/>
BY	
DISTRIBUTION/SECURITY CODES	
Dist.	AVAILABILITY SPECIAL
A	

UNCLASSIFIED

SECURITY CLASSIFICATION OF THIS PAGE(When Data Entered)

PREFACE

This is the final report of work performed at the Westinghouse Research & Development Center, Pittsburgh, Pennsylvania 15235 to determine the feasibility and scale-up potential of composite multi-spectral windows for use in airborne common-aperture electro-optic systems.

The work was accomplished under Contract No. F33615-76-C-5085 for the Laser Physics Branch, AFML/LPO under the guidance of Mr. David W. Fischer.

This report, submitted by the authors on 28 February 1977 is a summary of work done between 1 February 1976 and 31 January 1977. Dr. R. Mazelsky, Manager, Crystal Science & Technology Department, was the Project Supervisor and Dr. R. H. Hopkins was the Technical Program Manager. Mr. W. E. Kramer served as Principal Investigator and also directed the window development, fabrication and scale-up effort. Optical evaluation of the windows was performed by Mr. K. B. Steinbruegge and Dr. G. B. Brandt. Dr. R. A. Hoffman conducted the coating experiments and transmittance studies. Dr. J. S. Schruben performed some of the optical analyses.

We gratefully acknowledge the competent technical assistance of P. A. Piotrowski, E.P.A. Metz, R. F. Farich, D. M. Matusa, D. A. Yeager, C. Chamberlain, S. Pieseski, and B. Blankenship, without which the program would not have reached a fruitful conclusion.

TABLE OF CONTENTS

Section	Title	Page
I	INTRODUCTION	1
	1.1 Background and Objective	1
	1.2 Summary of Results	2
II	COMPOSITE WINDOW FABRICATION	3
	2.1 Composite Window Concept	3
	2.2 Optical Brazing	5
	2.3 Optical Cements	8
III	WINDOW MATERIAL SCREENING STUDIES	18
	3.1 Window Component Preparation and Evaluation	18
	3.2 Results of Initial Composite Evaluation	22
IV	CHARACTERISTICS OF OPTICALLY-BRAZED COMPOSITE WINDOWS	29
	4.1 Window Scale-Up	29
	4.2 Interferometric Evaluation	29
	4.2.1 General	29
	4.2.2 Interferometry of Window Components and Completed Composites	35
	4.3 Transmittance Studies	46
	4.3.1 General	46
	4.3.2 Transmittance of Uncoated Composite Windows	48
	4.3.3 Antireflective Coatings	52
	4.4 Thermophysical Properties	59
	4.5 Mechanical Properties	62
	4.5.1 Hardness and Strength of Window Components	62
	4.5.2 Bond Strength	62
	4.5.3 Rain Erosion Testing	62
V	CONCLUSIONS	68
	REFERENCES	70

LIST OF ILLUSTRATIONS

Figure	Title	Page
1	Schematic depiction of a composite multispectral window.	1
2	The range of glass stability in the As-S-Se system (after Reference 17) and typical compositions employed during this study.	6
3	Schematic illustration of pressing fixture for composite window fabrication.	7
4	Five micron thick As-S-Se glass layer bonding a ZnS cladding to a ZnSe substrate (the lines parallel to the interface are scratches created during polishing).	9
5	Transmittance vs. wavelength for NaCl-Aron Alpha 101-NaCl, 2.5 to 20 μm	11
6	Transmittance vs. wavelength for NaCl-Aron Alpha 101-NaCl, 2.5-20 μm	12
7	Optical transmittance of NaCl-M Bond 610-NaCl composite, 2.5-25 μm	13
8	Optical transmittance of NaCl-Loctite 307-NaCl composite, 2.5-25 μm	14
9	NaCl-2114 Glue-NaCl, Adhesive layer 2 μ	15
10	NaCl-2211 Glue-NaCl, Adhesive layer 5 μ	16
11	NaCl-epoxi-patch 0151-NaCl, adhesive layer 5 μ	17
12	Composite window fabrication and test screening sequence..	19
13	Photograph of a 4 x 6 in. ZnS plate placed between crossed polarizers. The structure, composed of columnar "grains" overlayed by random strain centers (crosses, e.g., like that at arrow) is typical of the ZnS we used. .	21
14	Cluster of inclusions at the origin of the strain center indicated by the arrow in Fig. 13.	23
15	Erosion specimen E-13, Irtran CaF ₂ clad to ZnSe with glass C. Note transverse cracks in the CaF ₂ formed due to thermal expansion mismatch between cladding and substrate. Bond is intact.	26
16	Irtran CaF ₂ clad to KCl with glass C. Cracks developed in the salt substrate due to the thermal expansion mismatch with the cladding. Fringes indicate area where bond began to delaminate after the cracking occurred. . .	27
17	A 2 x 2 in. optically-brazed composite window (#2-2-1) composed of a 0.060 in. ZnS layer clad to ZnSe with 50% S glass.	30

Figure	Title	Page
18	A 2 x 2 in. optically-brazed composite window (#2-2-2) formed by cladding a 0.070 in. ZnS layer to ZnSe with a 50% S glass.	30
19	A 2 x 2 in. optically-brazed composite window (#2-2-3) formed by cladding a 0.040 in. Irtran MgF ₂ layer to ZnSe with a 60% S glass.	31
20	A 2 x 2 in. optically-brazed composite window (#2-2-4) formed by cladding a 0.070 in. ZnS layer to ZnSe with a 50% S glass.	31
21	Optically-brazed 4 x 6 in. ZnS/ZnSe window (#4-6-1) ZnS cladding is 0.040 in. thick.	32
22	Optically-brazed 4 x 6 in. ZnS/ZnSe window (#4-6-2) ZnS is 0.080 in. thick.	32
23	Interferogram of ZnS sheet used for cladding composite window #2-2-1.	36
24	Interferogram of ZnSe substrate used in composite window #2-2-1.	36
25	Interferogram of composite window #2-2-1, ZnS clad to ZnSe with 50% S glass.	37
26	Interferogram of ZnSe for window #4-6-1. Origin at upper left hand corner just off photo. The x-axis points down and y-axis to right.	37
27	Interferogram of ZnS for window #4-6-1. Origin at upper right corner above photo; x-axis points down and y-axis to left.	38
28	Interferogram of completed 4 x 6 in. ZnS/ZnSe composite window #4-6-1. Origin at upper left hand corner; x-axis points down and y-axis to right.	38
29	Fringe order matrix for ZnS window. The y-axis is to the right (opposite the sense of the photograph in Fig. 27). The x-axis is pointing down.	42
30	Fringe order matrix for ZnSe window in the same orientation of the photograph of Fig. 26.	43
31	Fringe order of the sum of the fringes for ZnSe and ZnS pieces.	44
32	Fringe matrix of the composite window photographed in Fig. 28.	45
33	Fringe order matrix of corrected window.	47

Figure	Title	Page
34a	Transmittance vs. wavelength for a 0.032 in. thick slice of B glass; 0.6-2.5 μm (uncorrected for reflection)	49
34b	Transmittance vs. wavelength for a 0.032 in. thick slice of B glass; 2.5 to 20 μm (uncorrected for reflection) . .	50
35	Transmittance vs. wavelength for 0.060 in. ZnS layer bonded to ZnSe with glass B (No AR coating)	51
36	Transmittance vs. wavelength for a 0.050 in. thick CVD ZnS plate (No AR coating)	53
37	Transmittance of a ZnS/ZnSe composite formed by bonding a 0.015 in. thick ZnS plate to ZnSe (No AR coating)	54
38	Transmittance versus wavelength for a MgF_2 /ZnSe composite fabricated by joining a 0.010 in. Irtran MgF_2 layer to ZnSe with glass C	55
39a	Transmittance versus wavelength for a PbF_2 , AR coated ZnS/ZnSe composite window, 0.6 to 2.5 μm	57
39b	Transmittance versus wavelength for a PbF_2 AR coated ZnS/ZnSe composite window, 2.5 to 20 μm	58
40	Thermal conductivity of 50 and 60% S glass bonding agents from 190 to 380K.	60
41	Fracture surface of ZnS/ZnSe composite tested to failure in tension. The crack path passed primarily through the ZnSe substrate (light). The dark areas are material that spalled after testing.	64
42	Ring cracks formed in the ZnS cladding of a ZnS/ZnSe composite rain erosion specimen after exposure to the simulated rain field.	64

LIST OF TABLES

Table	Title	Page
1	Properties of Candidate Organic Optical Cements	10
2	Sources of Materials Used for Window Fabrication	24
3	Evaluation of Window Composites Fabricated from Various Substrates, Claddings, and Bonding Media	25
4	Material Refractive Indices	33
5	Thermophysical Properties of Substrates, Claddings and Glasses Used to Fabricate Composite Multispectral Windows .	61
6	Typical Mechanical Properties of Cladding, Substrates and Glasses Used to Fabricate Composite Windows	63
7	Rain Erosion Test Data for Representative Composites . . .	66

SECTION I

INTRODUCTION

1.1 Background and Objective

Future generations of airborne electro-optical systems are being designed with a common aperture for all sensor components -- TV, FLIR, and laser designator/ranger -- to minimize overall system cost and size and to maximize performance. So far, the deployment of these systems has been hindered, however, by the lack of a suitable window to shield the sensors from the environment. The window must be highly transparent from 0.5 to 12 μm , cheap to produce, and resistant to environmental attack, particularly high speed raindrop impingement. Clearly, the materials requirements are stringent, and in fact none of the monolithic broadband windows -- alkali halides, semiconductors or glasses -- possess all the necessary characteristics. Polycrystalline chemically vapor deposited (CVD) ZnSe^2 and ZnS^3 are promising candidates, but the former lacks rain erosion resistance while the latter exhibits light absorption at visible wavelengths.

A logical way to circumvent the inherent limitations of monolithic optical structures is to form a composite window which combines the most useful features of diverse optical materials while minimizing their respective deficiencies. The composite, or sandwich-window, formed by bonding a hard erosion-resistant cladding to a weaker, but highly transmissive, substrate would exhibit erosion resistance comparable to that of the protective layer with minimal loss in overall optical performance.

The primary objective of this study thus was to develop a composite window with the combination of optical and mechanical properties required for airborne common aperture systems. This involved

identification of materials suitable for the substrate, cladding and adhesive of the composite window, development of a fabrication technique and identification of the scale-up potential for the composite window.

1.2 Summary of Results

We have tested the composite window concept on nearly forty combinations of substrate, cladding and adhesive; the approach definitely appears feasible for fabricating rain-resistant multispectral windows. CVD-ZnS bonded to CVD-ZnSe via a technique we call optical brazing^{*} emerged from screening studies as the most promising sandwich window for systems applications. We have successfully fabricated both 2 x 2 in. and 4 x 6 in. ZnS/ZnSe windows to illustrate the scale-up potential of the method. The bonding technique is also versatile; for example, MgF₂/ZnSe windows were also readily made.

The optical homogeneity of the ZnS/ZnSe windows is compatible with systems applications. Computer analysis of interferograms indicated that residual optical path differences (OPD) as low as about 1/5 fringe (0.63 μ m) across the apertures of 2 x 2 in. ZnS/ZnSe windows could be obtained. Examination of interferograms taken from component window parts before assembly shows that most of the OPD variations were due to the material properties, not the joining process. Much of the path variation can be corrected by polishing. The transmittance of the composite windows is sufficiently good that with anti-reflective (AR) coatings they meet or exceed the minimum system specifications. Moreover, rain erosion tests verify that optically-brazed ZnS/ZnSe composites resist rain attack as well as ZnS alone. What remains to be demonstrated is that 14 x 20 in. windows, the size ultimately required for systems applications, can be made.

^{*} Patent applied for.

SECTION II

COMPOSITE WINDOW FABRICATION

2.1 Composite Window Concept

The composite window is conceptually simple: a thin, hard laminate is bonded to a conventional broadband window substrate, as depicted in Fig. 1. The joining may be accomplished in situ, e.g., by the direct chemical vapor deposition of ZnS on ZnSe as practiced by Raytheon,⁴ or by means of any bonding agent, or adhesive, which meets the transmittance requirements. We adopted the latter approach, a course of action facilitated by the Westinghouse-developed bonding technique, optical brazing,⁵ that is both versatile and simple to use. Note from Fig. 1 that the cladding layer need only be thick enough to protect the substrate; thus, even materials that exhibit low transmittance in thick sections can be used without impairing the transmittance of the composite. Further, there is no limitation in principle in the choice of materials that are used to form the composite. Hence, a variety of materials combinations are possible for tailoring the properties of the window and minimizing its cost.

The selection of a suitable substrate is based mainly on optical performance. For example, ZnSe and the alkali halides are among the few materials which transmit well from 0.5 to 12 μm in thick sections. Rain erosion resistance is the main criteria for cladding selection. Since impingement erosion imposes a unique loading condition which is not yet adequately understood, considerable theoretical and experimental effort has been expended recently to determine the mechanisms of rain erosion in transparent materials.⁶⁻¹⁷

The damage caused when a raindrop strikes a brittle window material derives from (1) the high pressure generated as the droplet

SECTION II

COMPOSITE WINDOW FABRICATION

2.1 Composite Window Structure

The composite window is conceptually similar to a film, which is bonded to a mechanical substrate window substrate, as indicated in Fig. 1. The window may be accomplished in situ, or the largest chemical vapor deposition of 100 to 120, as practiced by the use of an bonding agent, or otherwise, which means the window is bonded to the substrate.

Own. 6407A18

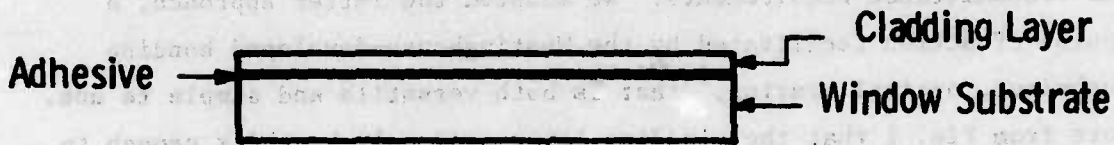


Fig. 1. Schematic depiction of a composite multispectral window.

is suddenly stopped and (2) the rapid lateral outflow of liquid as it escapes from the high pressure zone.¹⁴ When the droplet impact velocity exceeds a critical value, the tensile stresses generated in the window are sufficient to initiate failure or propagate pre-existing flaws. During continued rain exposure, the cracks grow and interact to form a distributed network. The transmittance is severely reduced by reflections at the window-crack interfaces so the window becomes effectively useless well before catastrophic failure occurs.

Semi-empirical rules suggest⁸⁻¹⁰ that erosion resistance improves with material hardness and ultimate strength. Although there may be mitigating factors in these relations,^{14,15} they can be used to guide cladding selection, recognizing, of course, that lattice absorption generally shifts to shorter wavelengths with increasing hardness¹ so that improved erosion resistance may be bought at the price of reduced transmittance.

2.2 Optical Brazing

Our studies indicate that chalcogenide glasses, particularly those from the As-S-Se system, are practical and versatile bonding agents. In addition, the refractive index, softening temperature, and thermal expansion coefficient of the glasses are composition-dependent¹⁷ so that the properties of the bond can be tailored somewhat to match those of the cladding and substrate. The glasses are stable over wide limits in the ternary system, Fig. 2.

In practice, a composite window is formed by the following simple sequence of operations performed with the aid of the apparatus illustrated in Fig. 3. The mating surfaces of each window component are polished flat and parallel (Section 3.2) and a 10 to 20 mil thick slice of glass is inserted between them to form a sandwich. The assemblage is heated (200-250°C) under fifty lbs per in² pressure. When warmed, the chalcogenide glass wets the materials to be joined and flows

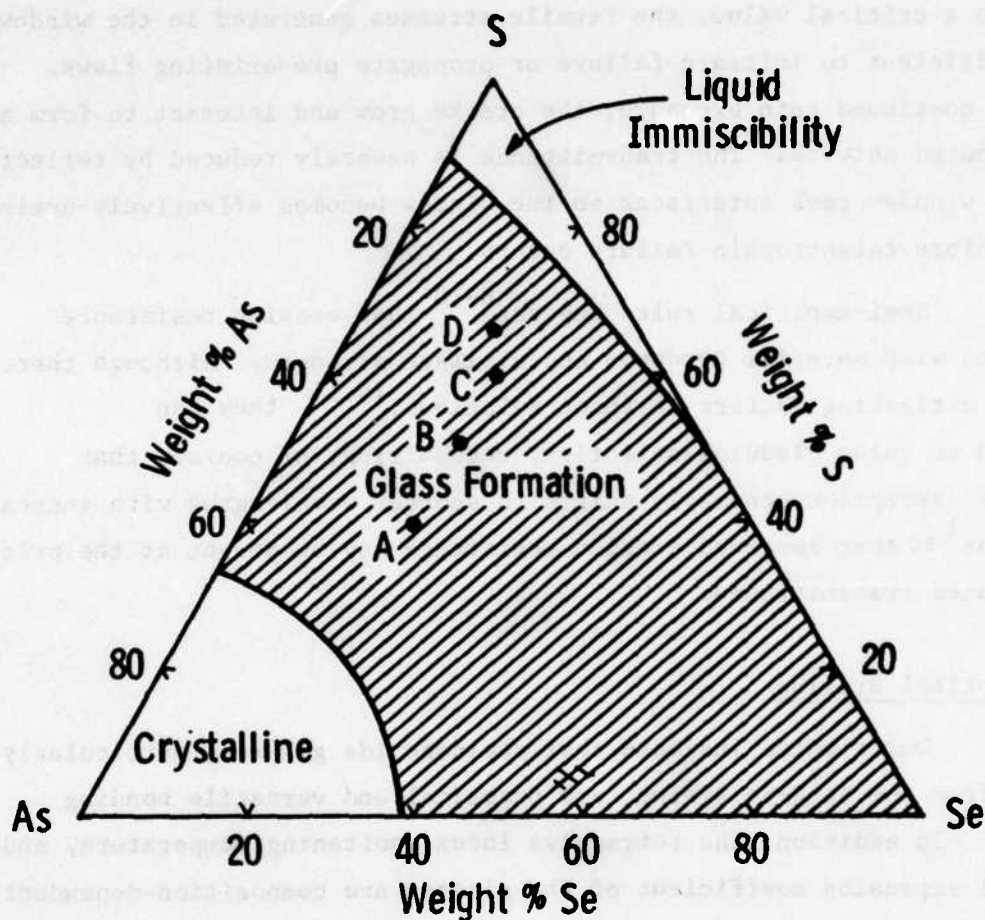


Fig. 2. The range of glass stability in the As-S-Se system (after Reference 17) and typical compositions employed during this study. Glasses are often referred to in the text by their sulfur content, e.g., glass C is the 60% S glass and glass B is the 50% S glass.

Dwa. 6407A17

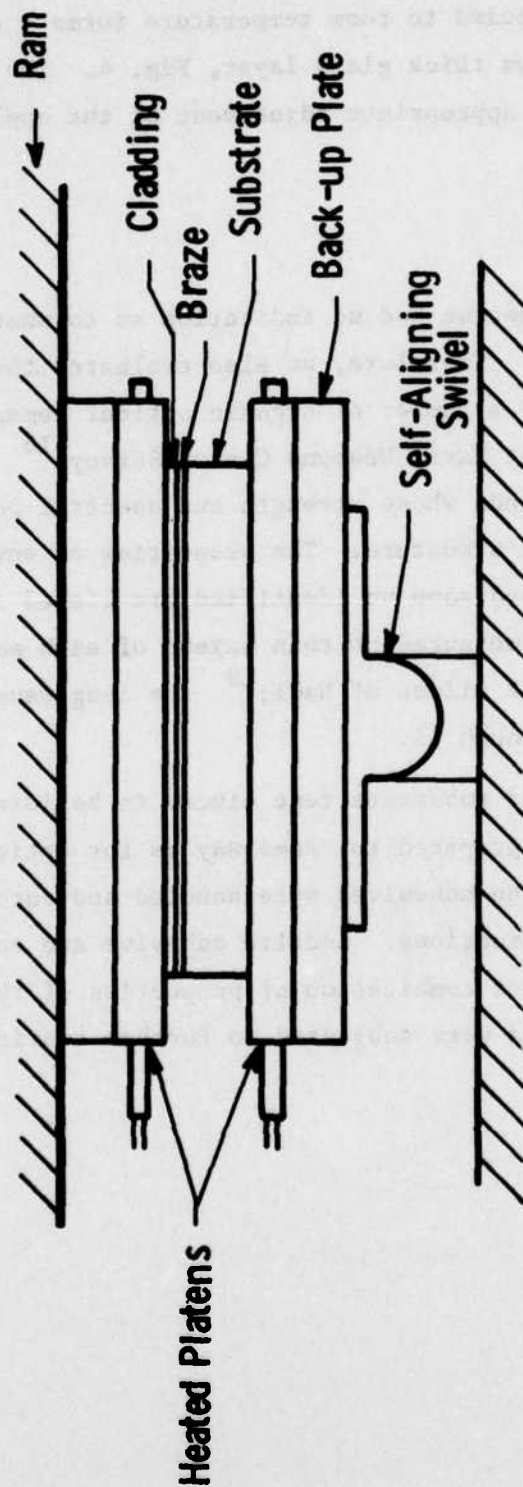


Fig. 3. Schematic illustration of pressing fixture for composite window fabrication.

to form a thin layer. As the glass is transparent, we termed the process "optical brazing" by analogy to conventional metal joining technology. The composite when cooled to room temperature forms a coherent structure joined by a 5 to 10 μm thick glass layer, Fig. 4. The layer thickness can be controlled by appropriate adjustment of the applied pressure and temperature.

2.3 Optical Cements

At the outset we had no indication as to what types of adhesives would prove optimal. Therefore, we also evaluated the utility for window fabrication of a number of organic optical cements like those identified in a recent Naval Weapons Center Survey.¹⁸ These compounds exhibit absorption bands whose strength and spectral position are sensitive to chemical structure. The properties of several of the suggested adhesives and some we identified are listed in Table 1. Transmittance curves were measured on thin layers of each material formed between two 5 mm thick slices of NaCl;¹⁸ the long wavelength spectra appear in Figs. 5 through 11.

Cladding and substrate test pieces to be joined with the optical cements were prepared the same way as for optical brazing (see Section 3.1). The adhesives were handled and cured according to manufacturers instructions. Loctite adhesive and epoxies 2114 and 2211 exhibited the best combination of properties of those materials listed in Table 1, and were subjected to further testing, Section 3.2.

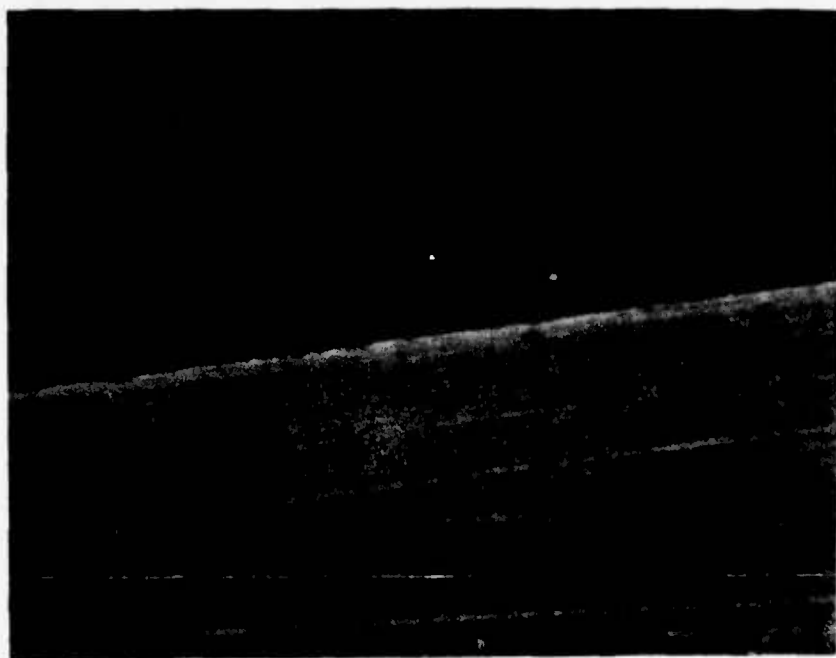


Fig. 4. Five micron thick As-S-Se glass layer bonding a ZnS cladding to a ZnSe substrate (the lines parallel to the interface are scratches created during polishing).

TABLE 1

Properties of Candidate Organic Optical Cements

Name	Manufacturer	Type	Cure	Color	Bond Characteristics	Visible	Transmittance* 1.06μ 8-12μ	(Fig)
Aron Alpha 101	Tongosei Chemical Co., Ltd	Cyanoacrylate 1 part system	RT 15 sec	Clear	Near instant adhesion Bubbles cannot be pressed out	90%	90% 80-90% Absorption Bands	5
Aron Alpha 102	Tongosei Chemical Co., Ltd	Cyanoacrylate 1 part system	RT 45 sec	Clear	Bubbles cannot be pressed out	85%	87% 45-80% Many Absorption Bands	6
M-Bond 610	Micro-Measurements Vishay InterTechnology	Epoxy 2 part system	160°C 2 hrs Pressure	Yellow	Bubbles form unless adhesive is pre-evaporated	80%	80% 0-65% Absorption Bands	7
Loctite 307	Loctite Corp.	1 Part Thick Industrial Adhesive	100°C Pressure	Clear	Bubbles difficult to press out - Erosion sample prepared	85%	88% 77-90%	8
TRA-BOND 2114	TRA-CON Inc.	Epoxy 2 part system	65°C 4 hrs Pressure	Clear	Fair adhesion - will delaminate if large mismatch in thermal expansion	87%	90% 70-88% Absorption Bands	9
TRA-BOND 2211	TRA-CON Inc.	Epoxy 2 part system	85°C 4 hrs Pressure	Amber	Good adhesion - cracks sample if large mismatch in thermal expansion	85%	88% 88-90%	10
Hysol #0151	Hysol Division The Dexter Corp.	Epoxy 2 part system	140°F 2 hrs Pressure	Clear	Difficult to get a uniform bond layer	75%	82% 85-90%	11

* Not corrected for reflective loss.

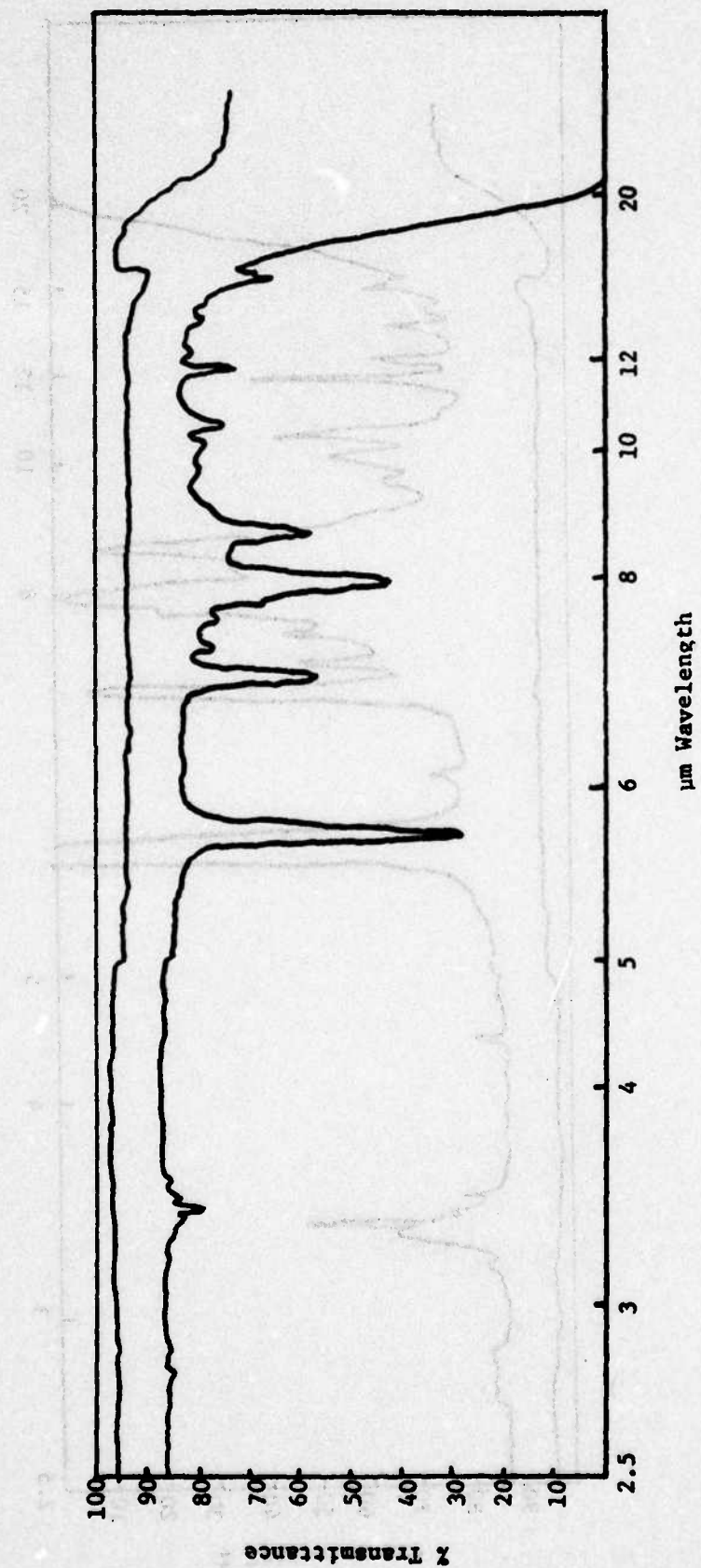


Fig. 5. Transmittance vs. wavelength for NaCl-Aron Alpha 101-NaCl, 2.5 to 20 μm .

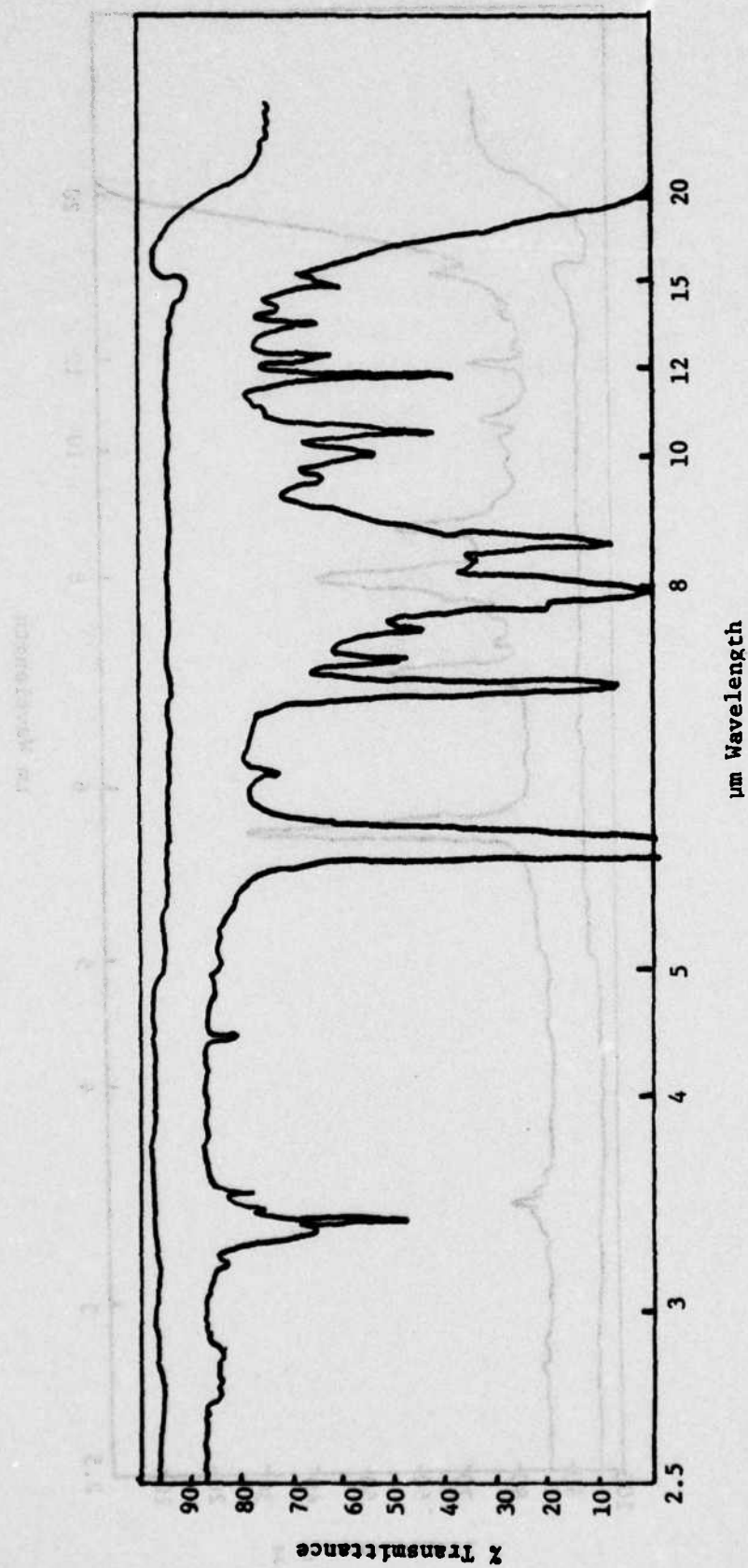


Fig. 6. Transmittance vs. wavelength for NaCl-Aron Alpha 102-NaCl, 2.5-20 μm .

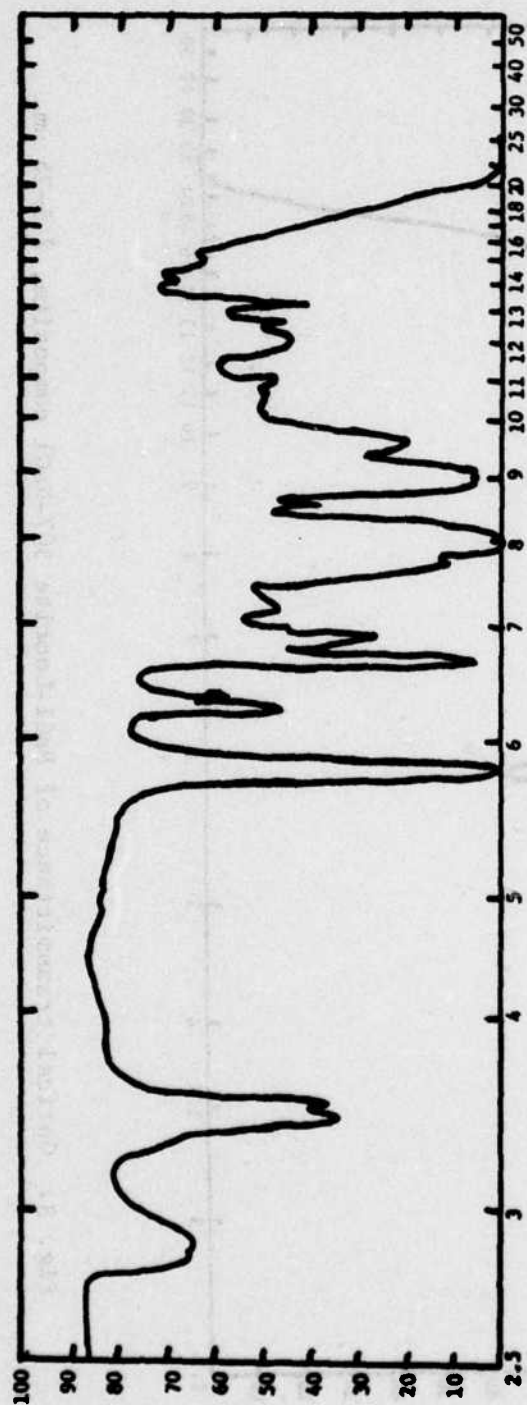


Fig. 7. Optical transmittance of NaCl-M Bond 610-NaCl composite, 2.5-25 μm .

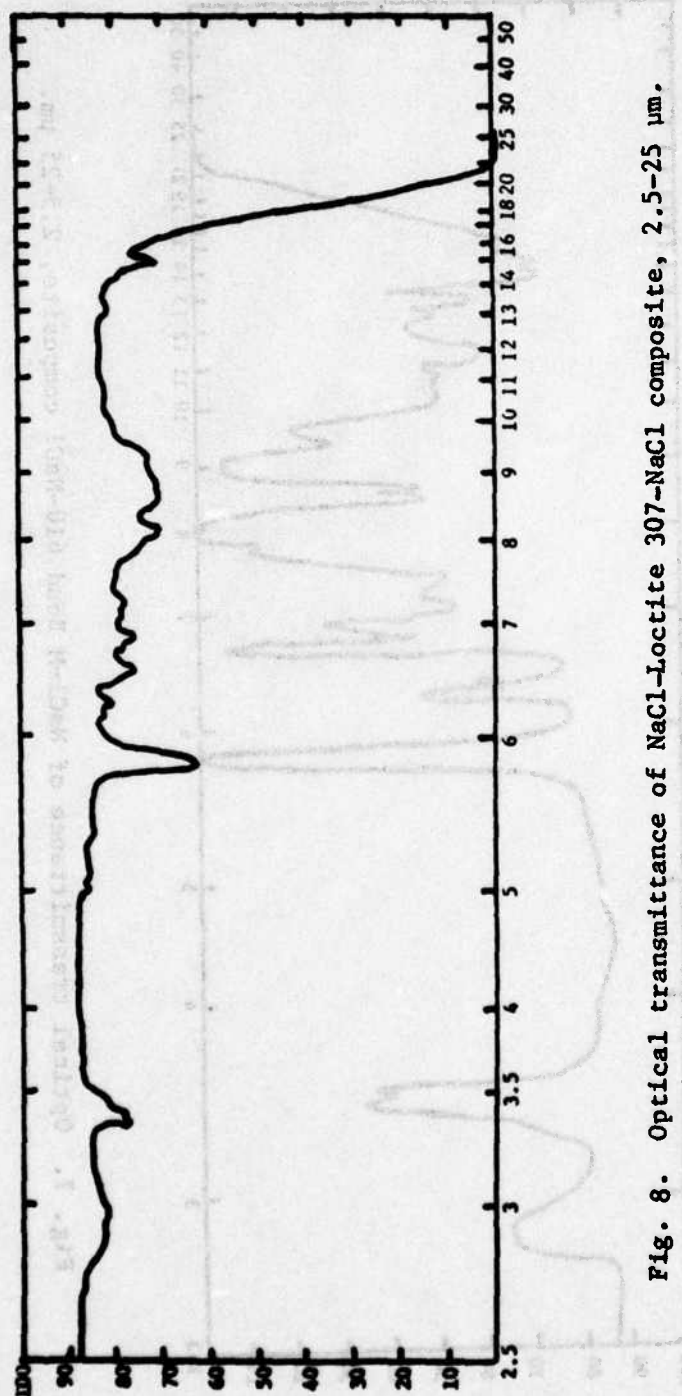


Fig. 8. Optical transmittance of NaCl-Loctite 307-NaCl composite, 2.5-25 μm .

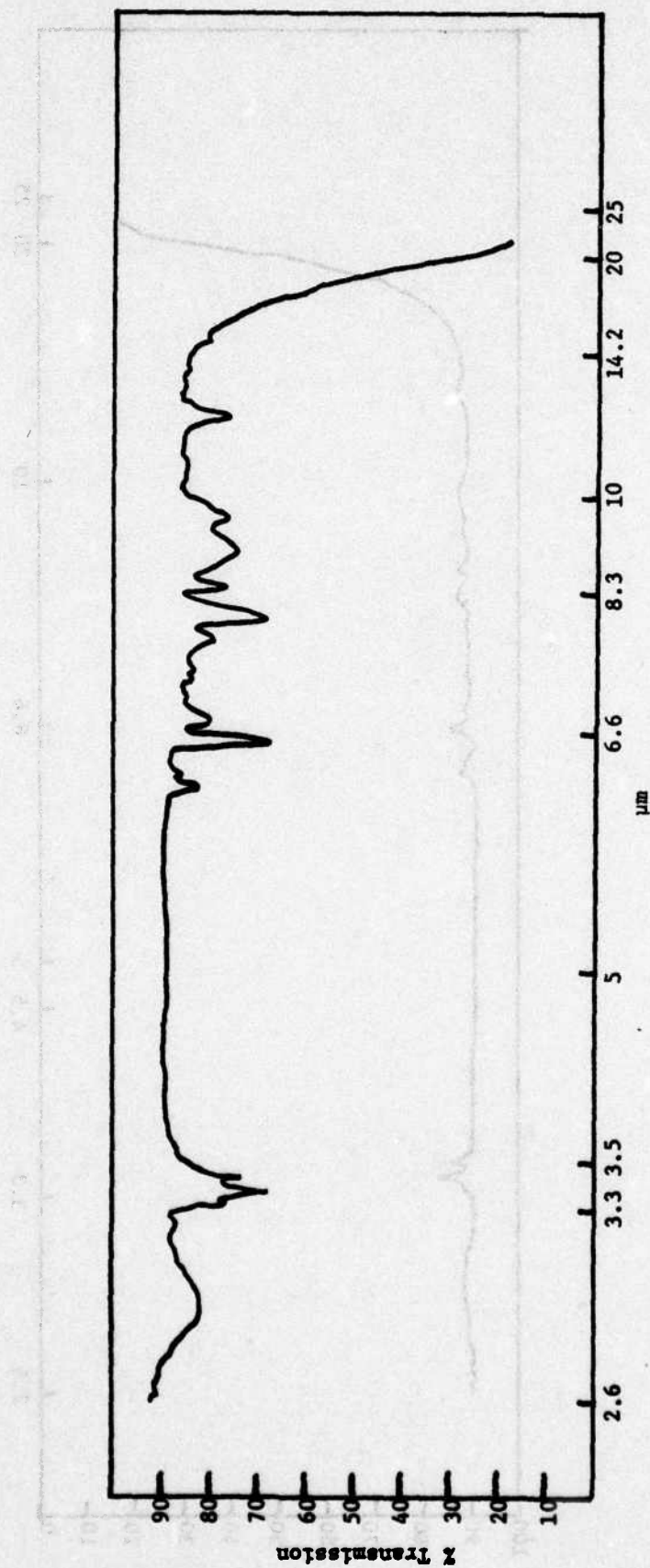


Fig. 9. NaCl-2114 Glue-NaCl,
Adhesive layer 2μ.

Fig. 8. NaCl-2211 Glue-NaCl,
Adhesive layer 5μ.

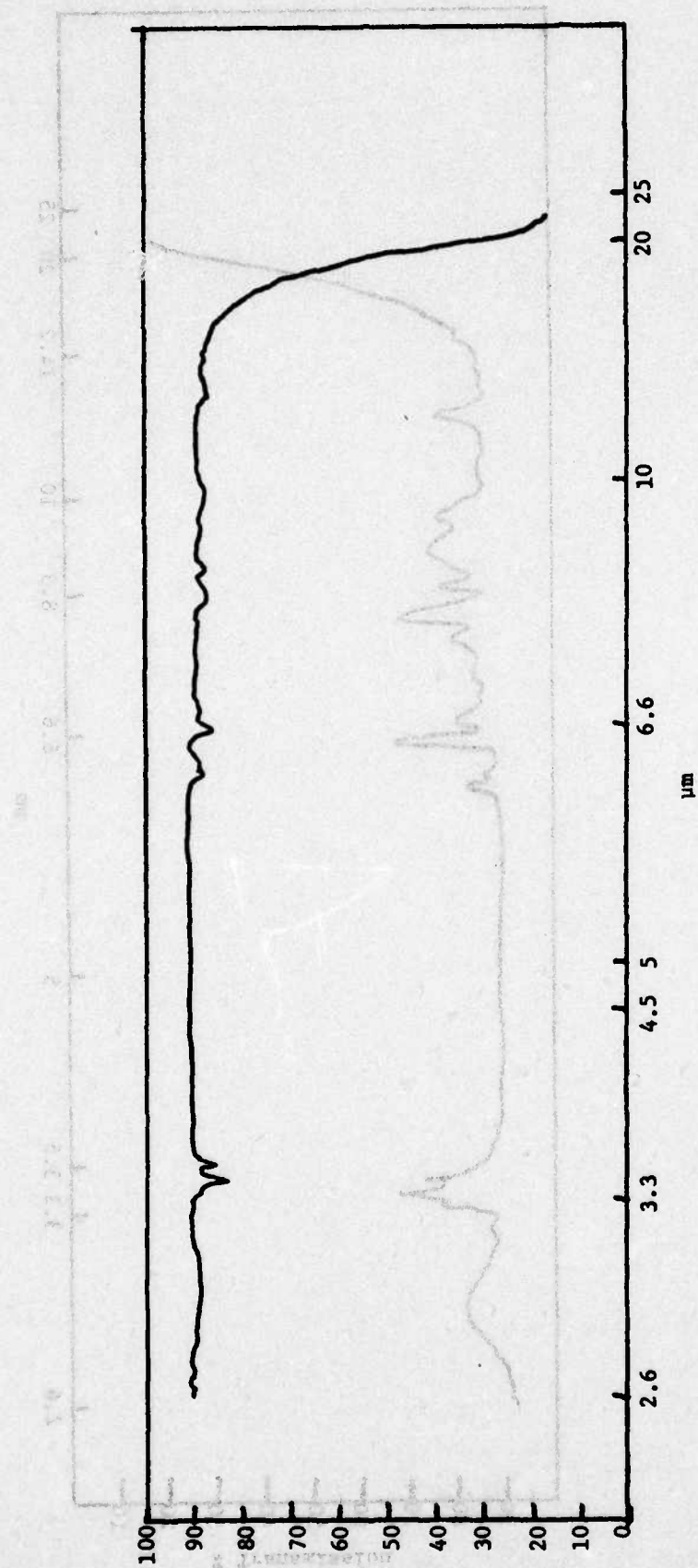


Fig. 10. NaCl-2211 Glue-NaCl,
Adhesive layer 5μ.

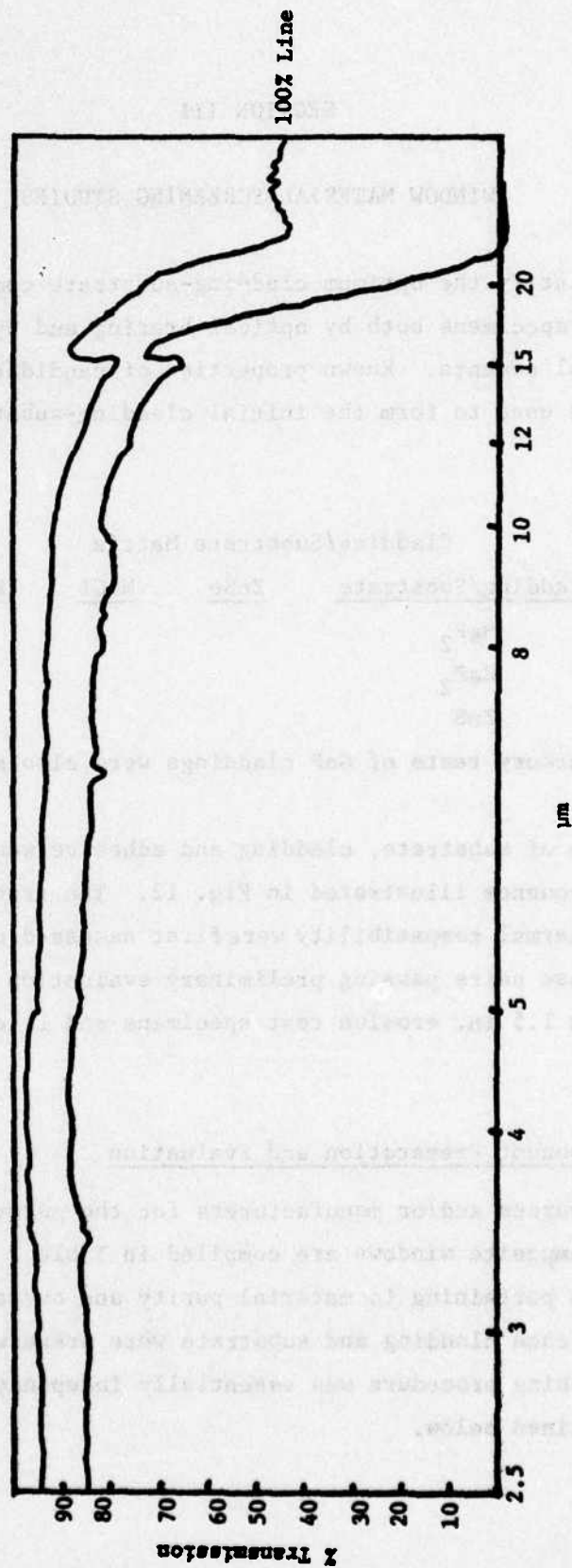


Fig. 11 NaCl-epoxi-patch 0151-NaCl
adhesive layer 5μ.

SECTION III

WINDOW MATERIAL SCREENING STUDIES

To identify the optimum cladding-substrate combination, we fabricated test specimens both by optical brazing and by using the most promising optical cements. Known properties of candidate materials (Section 4) were used to form the initial cladding-substrate matrix indicated below.

Cladding/Substrate Matrix			
<u>Cladding/Substrate</u>	<u>ZnSe</u>	<u>NaCl</u>	<u>KCl</u>
MgF ₂			
CaF ₂			
ZnS			

(Very cursory tests of GaP claddings were also made.)

Each combination of substrate, cladding and adhesive was subjected to the screening sequence illustrated in Fig. 12. The transmittance, bond integrity and thermal compatibility were first assessed on 0.5 x 0.5 in. test pieces; those pairs passing preliminary evaluation then were fabricated into 0.5 x 1.5 in. erosion test specimens and later into successively larger windows.

3.1 Window Component Preparation and Evaluation

The sources and/or manufacturers for the materials used to fabricate the composite windows are compiled in Table 2 along with some general comments pertaining to material purity and overall quality. Flat samples of each cladding and substrate were prepared in our optical shop. The polishing procedure was essentially independent of specimen size and is outlined below.

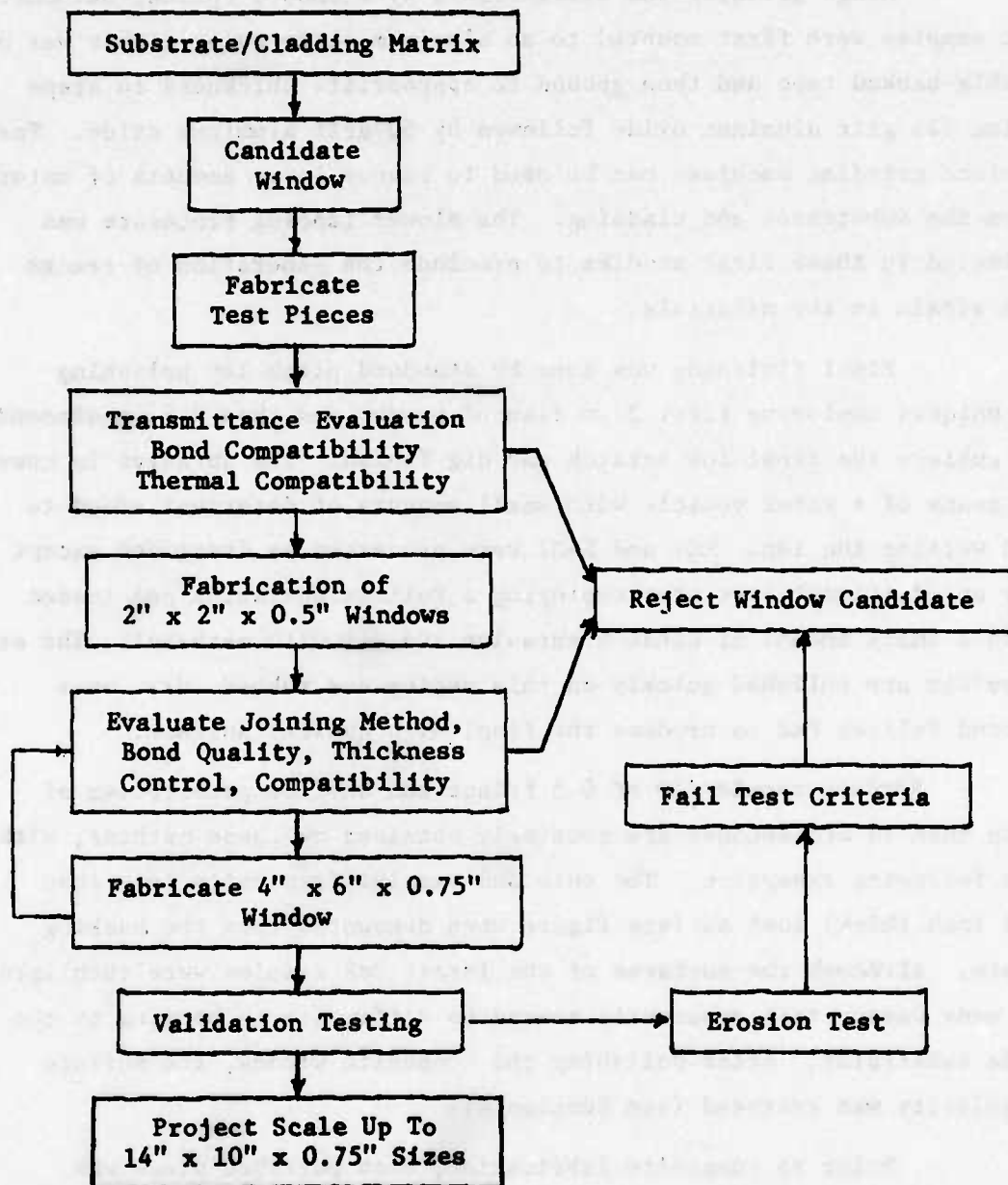


Fig. 12. Composite window fabrication and test screening sequence.

Rough grinding was accomplished by standard optical methods: the samples were first mounted to an aluminum plate using either wax or double-backed tape and then ground to appropriate thickness in steps using 225 grit aluminum oxide followed by 50 grit aluminum oxide. Faster surface grinding machines can be used to remove large amounts of material from the substrates and cladding. The slower lapping procedure was selected in these first studies to preclude the generation of cracks and strain in the materials.

Final finishing was done by standard pitch lap polishing techniques employing first 3 μm diamond powder and then 0.5 μm diamond to achieve the final low scratch and dig finish. The abrasive is conveyed by means of a water vehicle with small amounts of detergent added to aid wetting the lap. KCl and NaCl were processed as described except for an additional last step employing a Politex polishing pad loaded with a small amount of Linde A abrasive and wet with methanol. The salt crystals are polished quickly on this medium and rubbed dry on a second Politex Pad to produce the final high quality surface.

Surface regularity of 0.5 fringe and surface parallelism of less than 15 arc seconds are routinely obtained by these methods, with the following exception. The thin ZnS samples (typically less than 1/8 inch thick) lost surface figure when demounted from the backing plate. Although the surfaces of the larger ZnS samples were then irregular by many waves, this apparently caused no difficulty in bonding to the ZnSe substrates. After polishing the composite window, the surface regularity was restored (see Section 4).

Prior to composite fabrication, each polished piece was examined visually for overall homogeneity and under a polarascope to test for residual strain. The Irtran claddings exhibited some scattering, typical of other transparent hot-pressed materials, but were otherwise uniform. The CVD ZnS while visually homogeneous displayed considerable structure under polarized light, e.g., Fig. 13. The ZnS is composed of



Fig. 13. Photograph of a 4 x 6 in. ZnS plate placed between crossed polarizers. The structure, composed of columnar "grains" overlaid by random strain centers (crosses, e.g., like that at arrow) is typical of the ZnS we used.

a three-dimensional columnar "grain" structure overlaid at random by cross-marked strain centers (arrow). At each location in the ZnS where the cross patterns appeared, we detected clusters of inclusions like those in Fig. 14. These features were typical of all the CVD ZnS we examined. In contrast, the CVD ZnSe was generally devoid of light scattering and structure. Both the KCl and NaCl appeared inclusion-free and optically uniform.

3.2 Results of Initial Composite Evaluation

Composites were successfully produced from ZnS/ZnSe, MgF_2/ZnSe , CaF_2/ZnSe , ZnS/KCl, CaF_2/KCl , MgF_2/KCl , ZnS/KCl, CaF_2/KCl , MgF_2/KCl , and GaP/ZnSe in 0.5 x 0.5 in. size, confirming that optical brazing has general utility for joining transparent materials with dissimilar properties. The better organic cements also worked for many of the small composite test pieces.

As sample size was increased to 0.5 x 1.5 in. and larger, significant thermal incompatibility developed in many of the pairs and the composites failed as the data in Table 3 indicate. Specimens made from materials with the largest difference in thermal expansion coefficient, i.e., ZnS/KCl and ZnS/NaCl, sometimes delaminated near the edges. In most cases, the glass bond was so tenacious that, depending on the relative fracture resistance, either the cladding or substrates themselves fractured following specimen fabrication. The behavior of the CaF_2/ZnSe composite, Fig. 15, illustrates cladding failure; substrate failure occurred for almost all composites based on NaCl or KCl, e.g., Fig. 16.

We found the organic adhesives generally difficult to apply to larger specimens without bubble formation. While the organic compounds appeared to form good bonds, the adhesive layer thickness and uniformity was hard to control. Since the adhesive layer had to be kept thin to obtain the required transmittance, viz., Figs. 9 to 11, this put the method at a serious disadvantage for the proposed application. Moreover,



Fig. 14. Cluster of inclusions at the origin of the strain center indicated by the arrow in Fig. 13.

TABLE 2

Sources of Materials Used for Window Fabrication

	<u>Manufacturer</u>	<u>Comments</u>
CVD ZnS	Raytheon Co.	Pieces purchased 1/9/76, 4/27/76, 5/21/76 and 8/11/76. Material generally shows strain centers and columnar structure under crossed polaroids.
CaF ₂	Hawshaw Chemical Co.	Material very susceptible to cracking when handled. No composites could be successfully made.
	Irtran 3 Eastman Kodak Co.	Material more hazy, but more shock resistant, than Hawshaw CaF ₂ .
MgF ₂	Irtran 1 Eastman Kodak Co.	Hazy to visual inspection.
	Optovac, Inc.	Single crystal.
GaP	polycrystal prepared by Bridgeman growth	High free carrier absorption.
CVD ZnSe	Raytheon Co.	Government furnished material.
NaCl polycrystal	Harshaw Chemical Co.	
KCl polycrystal	Harshaw Chemical Co.	
As, S, and Se	American Smelting and Refining Co.	5-9s purity Used to make chalcogenide glass.

TABLE 3

Evaluation of Window Composites Fabricated From
Various Substrates, Claddings, and Bonding Media

Substrate	Cladding	Adhesive	Results
ZnSe	ZnS	50% S glass	OK
ZnSe	ZnS	60% S glass	OK
ZnSe	ZnS	2114 Epoxy	delaminates
ZnSe	ZnS	2211 Epoxy	bubbles
ZnSe	ZnS	Loctite	layer too thick
ZnSe	MgF ₂	50% S glass	delaminates
ZnSe	MgF ₂	60% S glass	OK
ZnSe	MgF ₂	2114 Epoxy	delaminates
ZnSe	MgF ₂	2211 Epoxy	delaminates
ZnSe	MgF ₂	Loctite	OK
ZnSe	CaF ₂	50% S glass	delaminates
ZnSe	CaF ₂	60% S glass	CaF ₂ cracks
ZnSe	CaF ₂	2114 Epoxy	CaF ₂ cracks
ZnSe	CaF ₂	2211 Epoxy	CaF ₂ cracks
ZnSe	CaF ₂	Loctite	CaF ₂ cracks
KCl	ZnS	50% S glass	delaminates
KCl	ZnS	60% S glass	delaminates
KCl	ZnS	2114 Epoxy	KCl cracks
KCl	ZnS	2211 Epoxy	KCl cracks
KCl	ZnS	Loctite	KCl cracks
KCl	CaF ₂	50% S glass	delaminates
KCl	CaF ₂	60% S glass	small pieces OK
KCl	CaF ₂	2114 Epoxy	OK
KCl	CaF ₂	2211 Epoxy	KCl cracks
KCl	CaF ₂	Loctite	KCl cracks
KCl	MgF ₂	50% S glass	KCl cracks
KCl	MgF ₂	60% S glass	KCl cracks
KCl	MgF ₂	2114 Epoxy	KCl cracks
KCl	MgF ₂	2211 Epoxy	KCl cracks
KCl	MgF ₂	Loctite	KCl cracks
NaCl	CaF ₂	60% S glass	OK in thick layers
NaCl	CaF ₂	50% S glass	NaCl cracks
NaCl	CaF ₂	2114 Epoxy	NaCl cracks
NaCl	CaF ₂	2211 Epoxy	NaCl cracks
NaCl	CaF ₂	Loctite	NaCl cracks
NaCl	MgF ₂	60% S glass	NaCl cracks
NaCl	MgF ₂	50% S glass	NaCl cracks
NaCl	MgF ₂	2114 Epoxy	NaCl cracks
NaCl	MgF ₂	2211 Epoxy	NaCl cracks
NaCl	MgF ₂	Loctite	NaCl cracks
NaCl	ZnS	60% S glass	delaminates
NaCl	ZnS	50% S glass	delaminates
NaCl	ZnS	2114 Epoxy	NaCl cracks
NaCl	ZnS	Loctite	NaCl cracks
NaCl	ZnS	2211 Epoxy	NaCl cracks
KCl	2114 Epoxy	----	sent for test

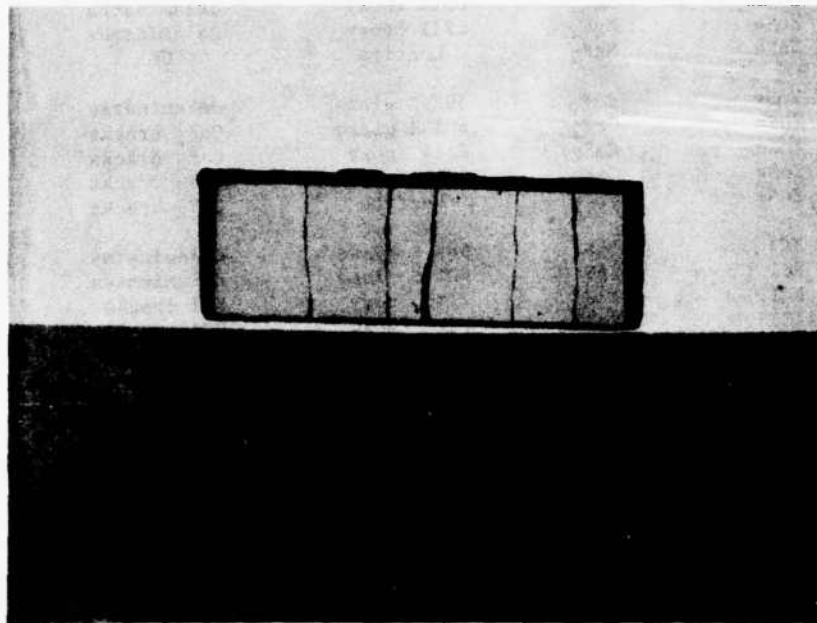


Fig. 15. Erosion specimen E-13, Irtran CaF_2 clad to ZnSe with glass C. Note transverse cracks in the CaF_2 formed due to thermal expansion mismatch between cladding and substrate. Bond is intact.

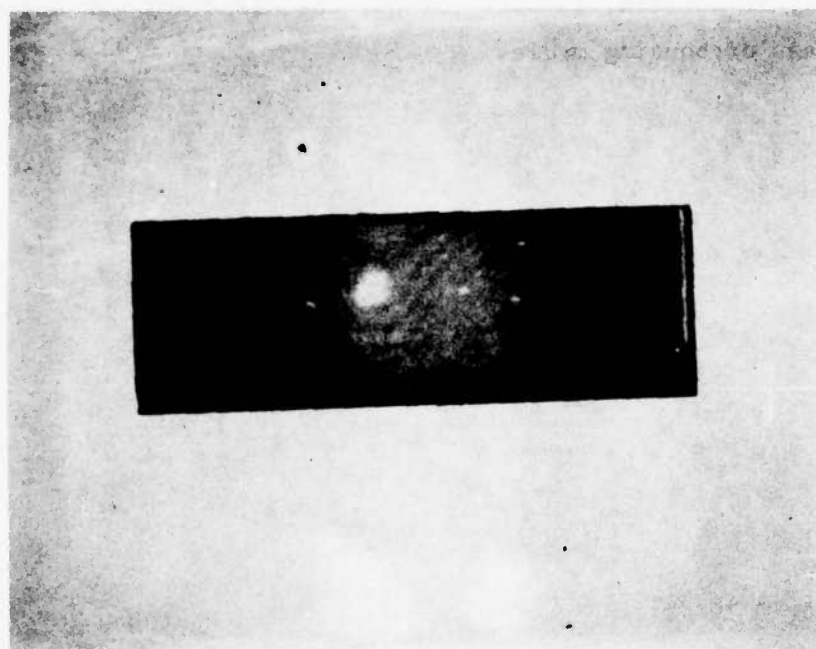


Fig. 16. Irtran CaF_2 clad to KCl with glass C. Cracks developed in the salt substrate due to the thermal expansion mismatch with the cladding. Fringes indicate area where bond began to delaminate after the cracking occurred.

specimen delamination was noted for the organically bonded composites subjected to rain erosion (Section 4.5).

The data in Table 2 indicate that of the pairs tested ZnS clad-ZnSe and $MgF_2/ZnSe$ are the most promising candidates for composite window fabrication. Optical brazing was the better joining method, the glass composition being adjusted somewhat depending on the particular materials to be bonded. Loctite exhibited the best combination of transmittance, joinability and durability of the organic cements we evaluated; it suffers, to some extent, the disadvantages noted above for that class of bonding media.

SECTION IV

CHARACTERISTICS OF OPTICALLY-BRAZED COMPOSITE WINDOWS

4.1 Window Scale-Up

Successful deployment of multispectral composites will require windows as large as 14 x 20 in. so it must be shown that the fabrication techniques are scalable to sizes greater than used for screening and erosion test pieces. The goal of this program was to achieve composite windows 2 x 2 in. and finally 4 x 6 in. in size. This has been successfully accomplished. A description of these windows and their properties follows below.

2 x 2 in. Windows. Screening studies suggested that the ZnS/ZnSe composite most closely fulfilled the optical and mechanical requirements for multispectral applications with the MgF_2/ZnSe window a potential alternative. We fabricated three 2 x 2 in. ZnS clad-ZnSe composites to develop scale-up techniques; a fourth 2 x 2 in. window was made from MgF_2 clad-ZnSe. Each window proved to be transparent, porosity-free and visually uniform as Figs. 17 through 20 indicate.

4 x 6 in. Windows. The 4 x 6 in. windows, Figs. 21 and 22, were made by the same procedure used for the smaller windows. As before, the joint between the cladding and substrate was pore-free, thin, and tenacious. There was no apparent thermal incompatibility in going from the 2 x 2 in. to 4 x 6 in. ZnS/ZnSe window. We did not attempt to make 4 x 6 in. MgF_2/ZnSe because of the relatively poorer optical properties exhibited by this combination, viz., the following sections.

4.2 Interferometric Evaluation

4.2.1 General

A major part of this program was to determine whether the optical brazing technique introduces any undesirable optical deviations



Fig. 17. A 2 x 2 in. optically-brazed composite window (#2-2-1) composed of a 0.060 in. ZnS layer clad to ZnSe with a 50% S glass.

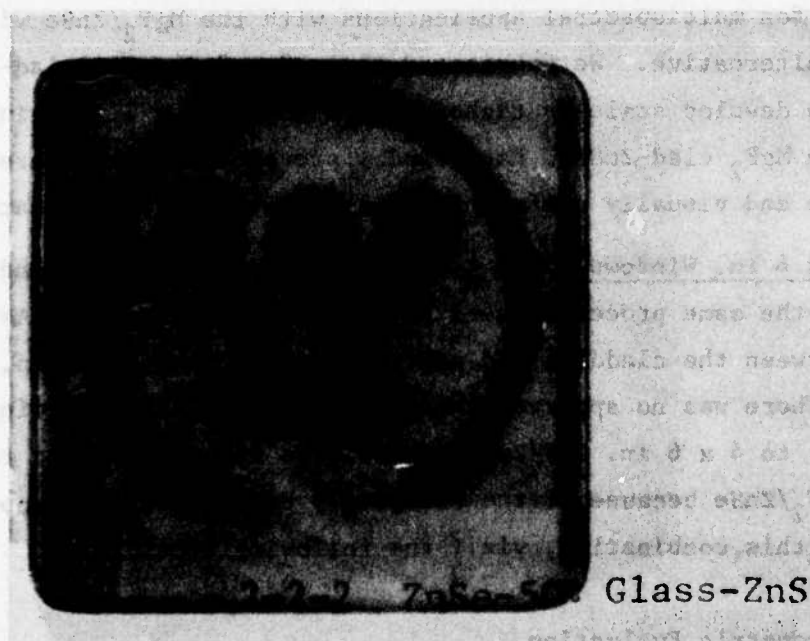


Fig. 18. A 2 x 2 in. optically-brazed composite window (#2-2-2) formed by cladding a 0.070 in. ZnS layer to ZnSe with a 50% S glass.

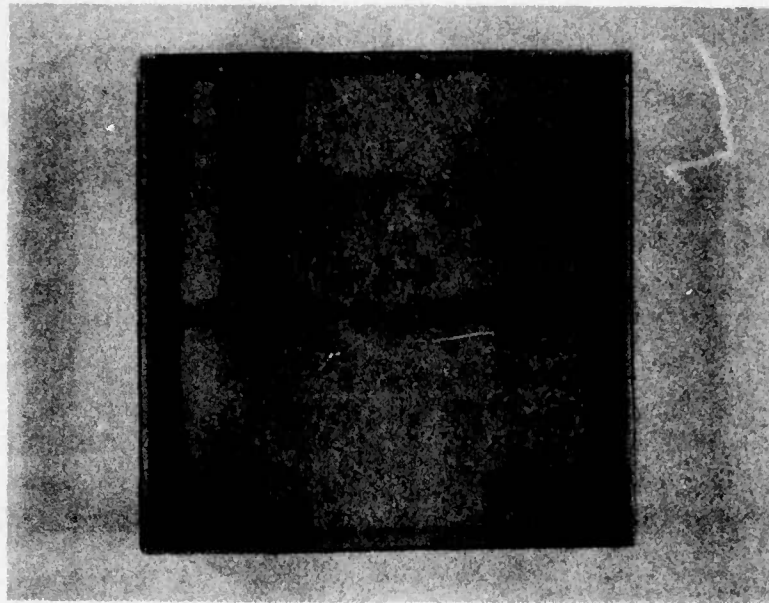


Fig. 19. A 2 x 2 in. optically-brazed composite window (#2-2-3) formed by cladding a 0.040 in. Irtran MgF_2 layer to ZnSe with a 60% S glass.

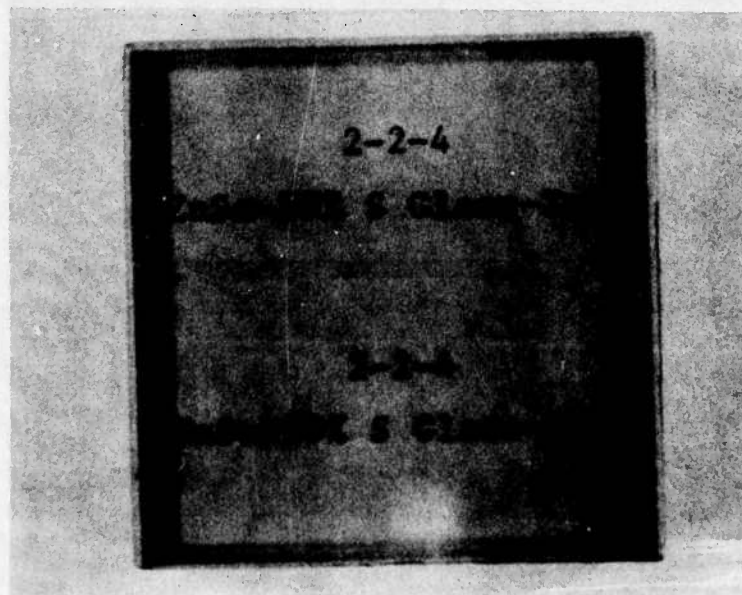


Fig. 20. A 2 x 2 in. optically-brazed composite window (#2-2-4) formed by cladding a 0.070 in. ZnS layer to ZnSe with a 50% S glass.



Fig. 21. Optically-brazed 4 x 6 in. ZnS/ZnSe window (#4-6-1) ZnS cladding is 0.040 in. thick.



Fig. 22. Optically-brazed 4 x 6 in. ZnS/ZnSe window (#4-6-2) ZnS is 0.080 thick.

into the window structure which were not already present in the starting material. Apart from scattering, optical path differences through an optical element are the most important influence on the image quality of a system containing that element. Sources of optical path difference are irregularities in the interface between two materials of different refractive index and changes in refractive index of the bulk material itself. Optical path differences induced by thickness or dimensional changes between two media are proportional to the amount of dimensional change, Δt , and the refractive index difference $(n_1 - n_2)$ across the interface. At a given wavelength λ , the number of wavelengths, N , that an interference pattern will be displaced by a given OPD is given by

$$N = (n_1 - n_2) \Delta t / \lambda .$$

Thus, the surface figure is most important where the refractive index difference is greatest, namely, between the outer window surface and air. Table 4 lists the values of refractive index for the various materials used to fabricate the windows at the three wavelengths of interest.

TABLE 4
Material Refractive Indices

Material	0.6328 μm	1.06 μm	10.6 μm
ZnS	2.26	2.25	2.20
ZnSe	2.57	2.48	2.40
Bonding* Glass	2.20	NA	NA

* Estimated from reflectivity data, Section 4.3.

From these data, it is clear that irregularities in the surface between the ZnS and the chalcogenide bonding glass are relatively unimportant since the refractive indices of the two materials are close.

At 0.6328 μm , an irregularity of one wavelength in the figure of the ZnSe surface is over five times worse than for the same irregularity between the bonding glass and ZnSe. This is because the refractive index difference is 1.57 in the first case and it is only 0.37 in the second. As a result, by its very nature, the optical brazing technique is not expected to introduce large optical path differences across the bonding joint. If the surface figure is good, as can be checked easily with conventional polishing shop methods, then the remaining influence of the window on optical system performance is limited to that which is introduced by compositional and refractive changes in the materials themselves.

Optical path itself does not influence image quality, but rather what is more important is the spatial variation of the OPD. A gradually varying OPD has little effect on imaging systems but a rapidly varying excursion can be very damaging to image quality. As an extreme example of the latter case, a shower glass is virtually useless as a window because of the short spatial variation of the optical path. In our analysis we have tried to handle the data in a manner which reduces the gradual variations so that we can better estimate the rapid changes in OPD.

For example, if a window is wedged, there is an optical path difference whose magnitude is

$$\text{OPD} = (n_1 - 1) \theta L/\lambda$$

where θ is the angle of the wedge and L the distance along it measured from the vertex. This OPD gradient, whether it be caused by dimensional or refractive index gradients can always be compensated by grinding a thin wedge in one of the optical surfaces. Similarly, a circular variation in optical path corresponding to a weak lensing effect, can be compensated by grinding a spherical surface on one face of the window. The damaging OPD variations are those which cannot be compensated. We

have, in the data reduction, chosen to subtract the wedge and spherical variations in order to illustrate the random variations in OPD which could be expected to influence image quality.

4.2.2 Interferometry of Window Components and Completed Composites

At the beginning of the fabrication process for the 2 x 2 in. windows, and throughout the subsequent portions of this program, interferograms were routinely made of the component materials both before and after they were formed into a completed composite window. An example of one sequence of these interferograms is illustrated in Figs. 23, 24, and 25 where the optical homogeneity of the ZnS, ZnSe, and the completed window, respectively, can be compared. From Fig. 23, it is evident that in addition to the wedge in OPD there is a significant spherical variation of several wavelengths at $0.6328 \mu\text{m}$. This variation is not due to surface figure (which was flat to $\lambda/4$) but rather due to refractive index variations in the material itself. The interferogram of the completed window in Fig. 25 shows the same behavior, indicating that the bonding process has at least not introduced any large changes in the OPD compared to those in the starting materials.

Figures 26, 27, and 28 show a similar set of interferograms for the components and the first completed 4 x 6 in. window. Due to the larger diameter, the material variation in refractive index is much greater. In the case of the thicker ZnSe, the OPD forms a gradual "hill" in one corner of the window (Fig. 26) which is also apparent in the final window. These variations are attributed to refractive index changes in the material since in both cases the surfaces were flat to better than one half wave. For the thinner ZnS (Fig. 27), the problem is complicated by the fact that the interferograms of the unmounted piece shows a saddle-shaped structure which does not appear in the final window. This is probably because the two sides of this thin piece were ground and polished separately with a demounting step in between. Even though the first face is flat to a fraction of a wave, it is difficult

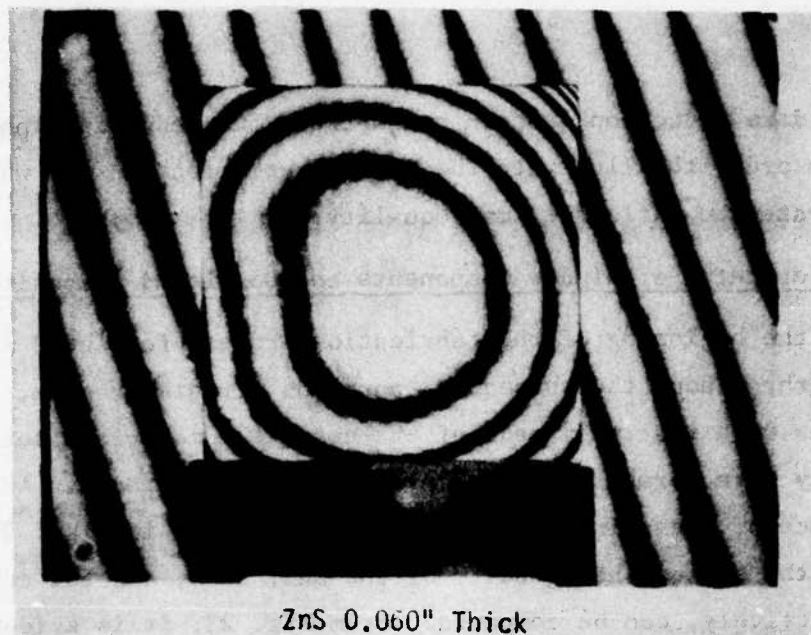


Fig. 23. Interferogram of ZnS sheet used for cladding composite window #2-2-1.

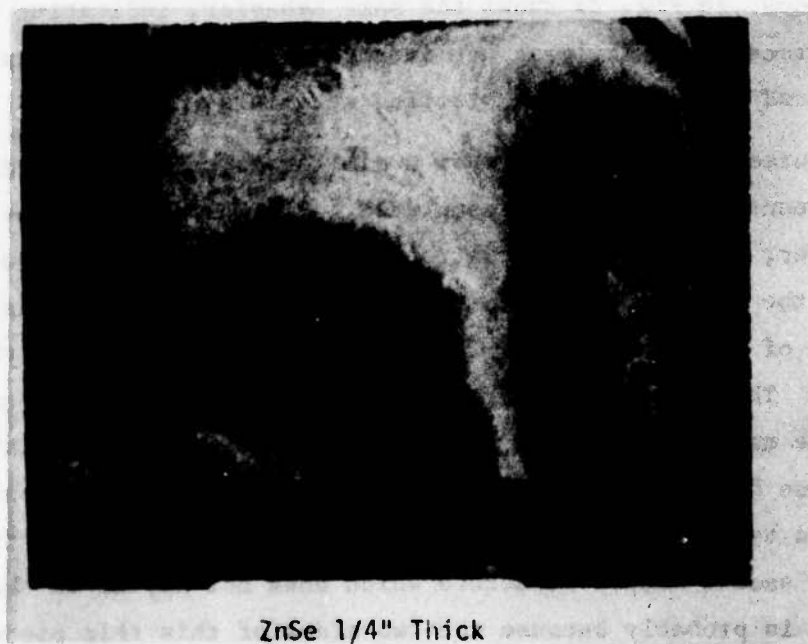


Fig. 24. Interferogram of ZnSe substrate used in composite window #2-2-1.



Fig. 25. Interferogram of composite window #2-2-1, ZnS clad to ZnSe with 50% S glass.

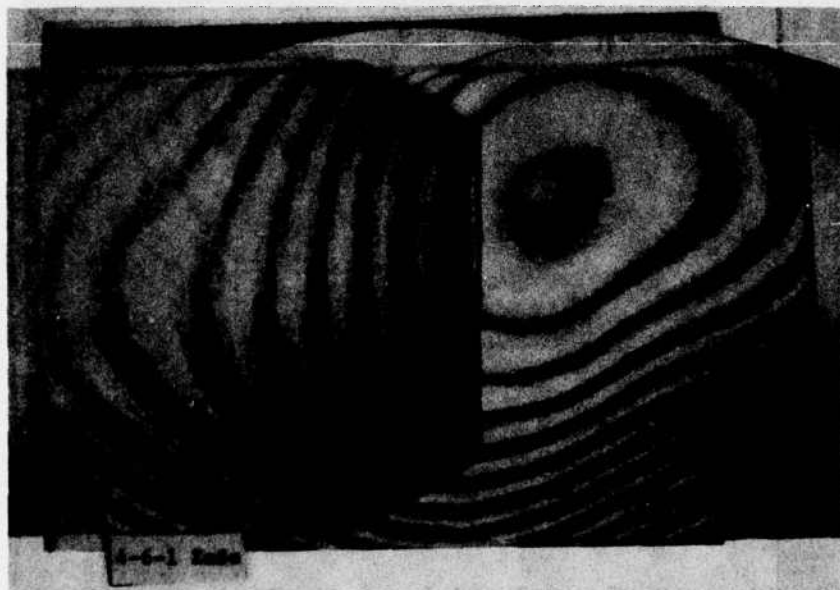


Fig. 26. Interferogram of ZnSe for window #4-6-1. Origin at upper left hand corner just off photo. The x-axis points down and y-axis to right.

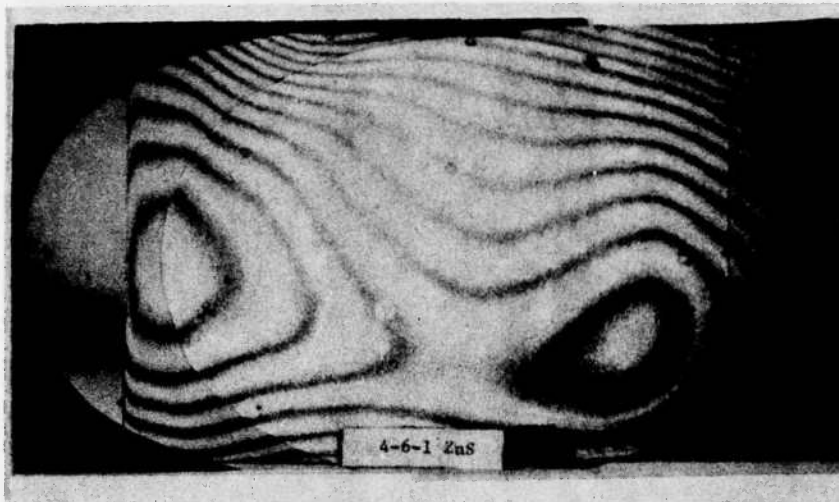


Fig. 27. Interferogram of ZnS for window #4-6-1. Origin at upper right corner above photo; x-axis points down and y-axis to left.

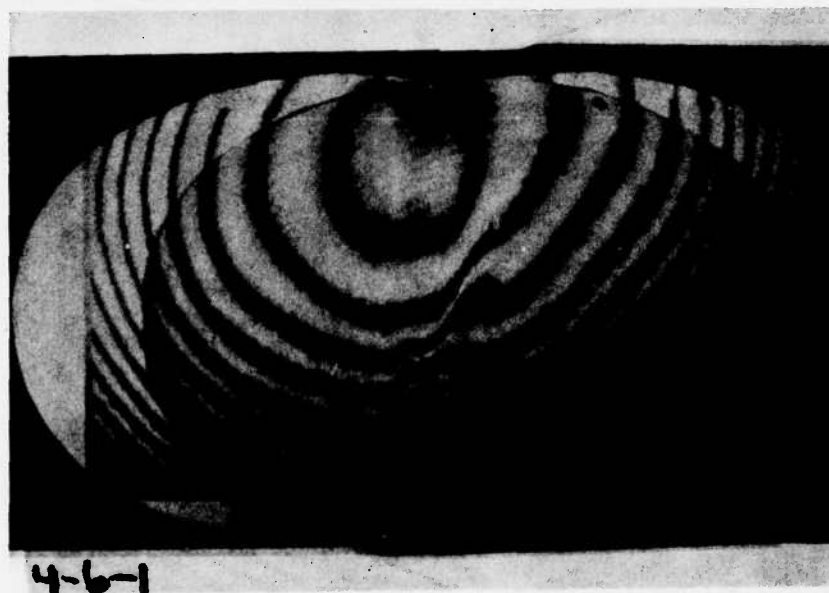


Fig. 28. Interferogram of completed 4 x 6 in. ZnS/ZnSe composite window #4-6-1. Origin at upper left hand corner; x-axis points down and y-axis to right.

to retain this flatness during the remounting to polish the second side. Thus as a result, we suspect the ZnS varied slightly in thickness across its diameter. This variation, however, was apparently removed in the final polishing step of the composite window structure since it does not appear in Fig. 28. It is easy to rule out the possibility that warping of the ZnS in the interferometer is the cause of the additional fringes which form the saddle in Fig. 27. As a parallel plate of thickness, t , is tilted in the interferometer, it increases the optical path through it. Thus, if the edges of the plate are warped to an angle θ relative to the center, an increased OPD equal to

$$\text{OPD} = t \cdot \theta^2 / 2n\lambda$$

results. If the ZnS were warped by an amount equal to its thickness (which it was not), this would produce an OPD of only 0.75 fringe. Thus, we conclude that a combination of refractive index variation and a slight thickness change in the ZnS is responsible for the fringe pattern in Fig. 27. The ZnSe and the completed sandwich window are much thicker than the ZnS so that warping between polishing of the two sides is less a problem. Thus, in both Figs. 26 and 28, the fringe pattern is due to index inhomogeneities in the material.

One feature which deserves notice in Fig. 28 is the discontinuity of the fringe pattern near the middle of the window. This indicates either a refractive index change of the bonding glass of 0.1 or a thickness change of the layer of about 2 μm . Since nothing can be seen visually in this region, the former is the more likely explanation for the artifact in the interferogram.

The interferograms of the MgF_2 , ZnSe, and the MgF_2/ZnSe composite indicated much higher fringe counts in this window than in the ZnS/ZnSe window. The high fringe content stemmed mainly from difficulties incurred when polishing the MgF_2 cladding. Several repolishings of the MgF_2 failed to reduce the piece to the required flatness since the slab warped

repeatedly on dismounting from the back plate. The piece also contained considerable scatter and a large blemish. Thus, while optical brazing of the MgF_2/ZnSe windows presented no apparent difficulty as Fig. 19 suggests, further polishing studies are required to produce distortion-free composites of these materials.

Our observations suggest the following important points which should be considered when scaling the fabrication process to larger windows. First, inhomogeneity in material refractive index is a problem if diffraction limited performance is to be obtained. Fortunately, much of the variation in material properties appears to be gradual which, in principle, can be corrected by changing the figure of the window's surface. The second point involves the mounting and polishing of large, thin sections such as the ZnS. Considerable care must be given to the mounting process; if the cladding has to be very thin, it may be difficult to guarantee perfect flatness or parallelism without special preparation.

4.2.3 Reduction of Interferometric Data

To get a measure of the "random" phase deviations of these windows which can be expected to influence the imaging of systems placed behind them, we have digitized the interferograms in Figs. 26 to 28 and have used a computer program to interpolate the OPD on a uniform grid over the aperture of the window.

First we examined the effect of combining the ZnS and the ZnSe layers by adding their individual fringe patterns and comparing this with the interferogram of the composite window. The interferograms can most easily be measured in the middle of each fringe. Since the fringes of two interferograms are in different locations so are the data points on the x-y plane of the window. In order to add the fringe orders, we interpolated the data on a common grid. This was done with a 1.0 cm grid spacing in the long edge of the window (y-direction) and 0.6 cm spacing along the shorter edge (x-direction). The grid size is 16 by 16 and is centered on the interferograms.

We used parabolic interpolation in the x-direction and then again in the y-direction. The resultant matrices of fringe orders are shown in Figs. 29 and 30 for ZnS and ZnSe respectively. The contour lines sketched in the figures represent the center of the white fringes in the interferograms. Figure 31 represents the addition of the matrices from Figs. 29 and 30. Ten fringe orders have been subtracted to facilitate comparison with the fringe matrix of the composite window (Fig. 32) since the fringe orders were not measured absolutely. Figures 31 and 32 are similar in contour; the one only peak is shifted from one figure to the other. As noted above, we do not expect the figures to be identical. What remains to be determined is the extent to which the composite window can be corrected by prism and spherical optics.

A wedge centered at angle θ from the x-axis towards the y-axis with a wedge angle α and a sphere centered at (x_0, y_0) with radius R would cause a fringe order N given by the equation:

$$\lambda N / (n-1) = \sqrt{R^2 - \rho^2} - R + \tan \alpha (x \cos \theta + y \sin \theta) + C,$$

where

$$\rho^2 = (x - x_0)^2 + (y - y_0)^2$$

and C is a constant which accounts for the relative nature of the fringe order measurements and the thickness of the window which is assumed to be taken into account in the final optical design. We took $n = 2.57$ and $\lambda = 0.6328 \mu\text{m}$. The results for the other wavelengths can be found by scaling. A modified Levenberg-Marquardt algorithm was used to find the values of the six parameters x_0 , y_0 , R , α , θ , C which minimize the root mean square of the fringe order matrix for the difference between the window fringes and the prism and sphere fringes. Since R is very large, only the first three terms of the Taylor series expansion of $\sqrt{R^2 - \rho^2}$ about $\rho = 0$ were used in order to improve numerical accuracy. Also, by considering only the first two terms in the expansion, a linear optimization problem could be formulated and solved to get the initial

DATE 021077

WINDOW INTERPOLATE

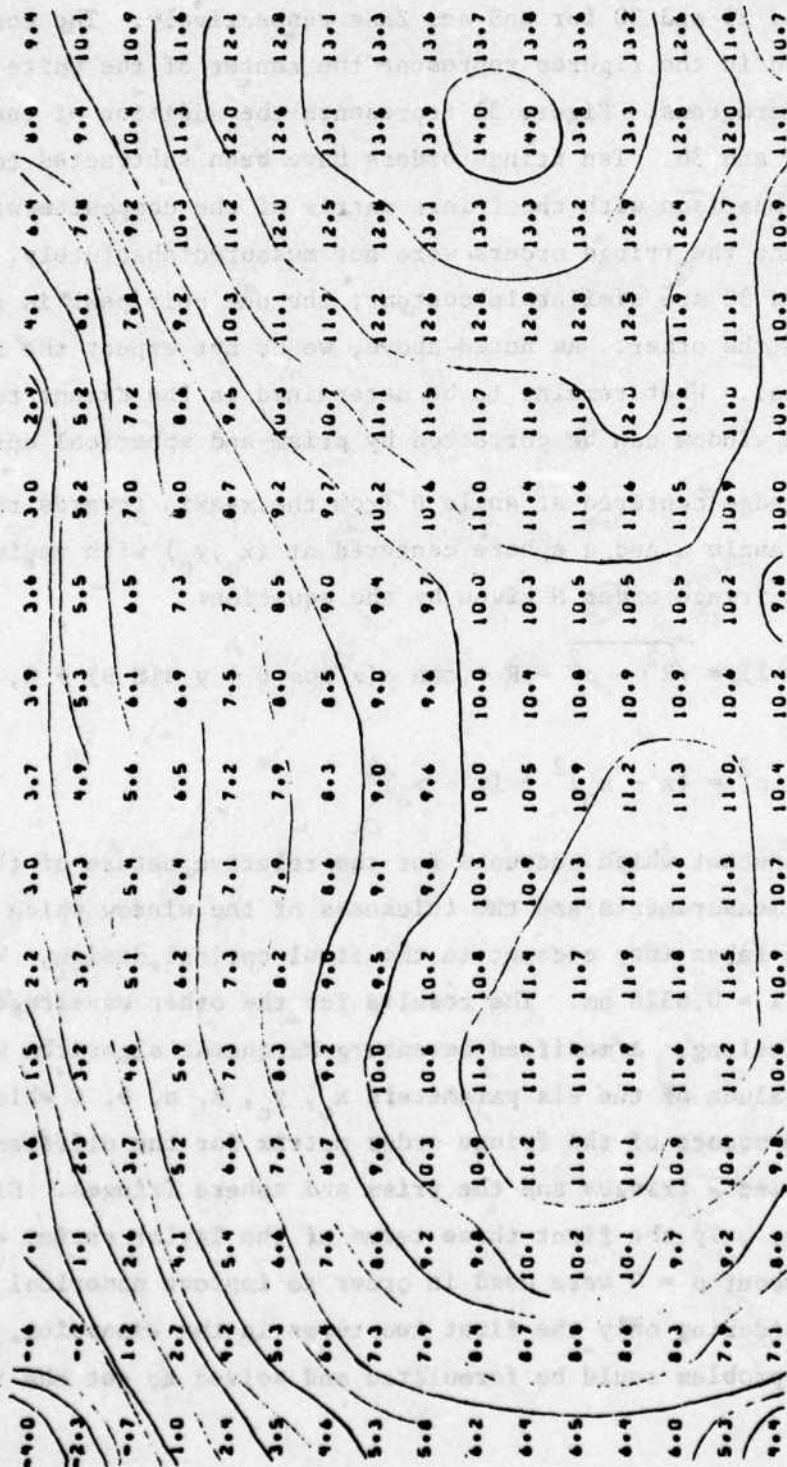


Fig. 29. Fringe order matrix for ZnS window. The y-axis is to the right (opposite the sense of the photograph in Fig. 27). The x-axis is pointing down.

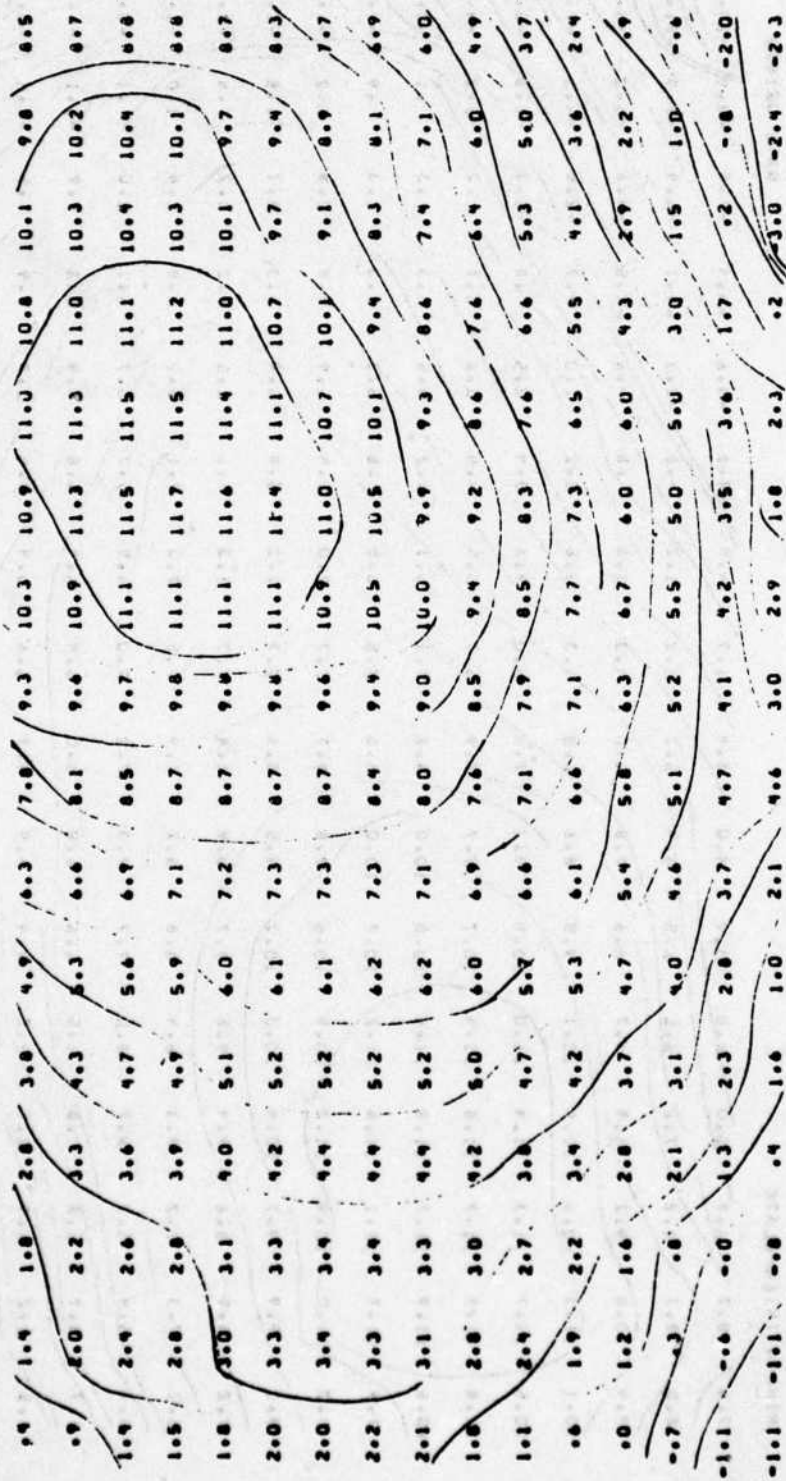


Fig. 30. Fringe order matrix for ZnSe window in the same orientation of the photograph of Fig. 26.

DATE 021077

BINDING INTERPOLATE

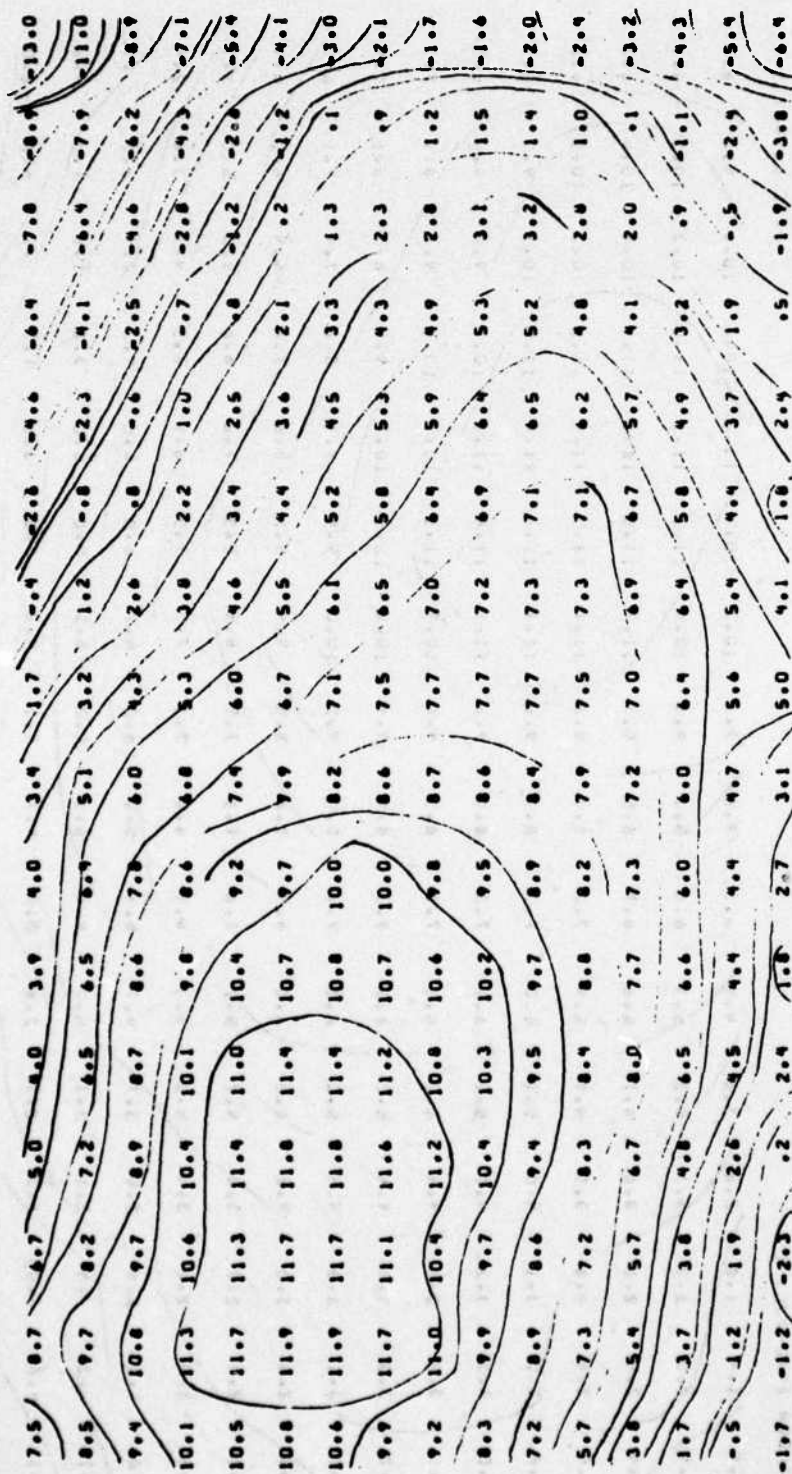


Fig. 31. Fringe order of the sum of the fringes for ZnSe and ZnS pieces.

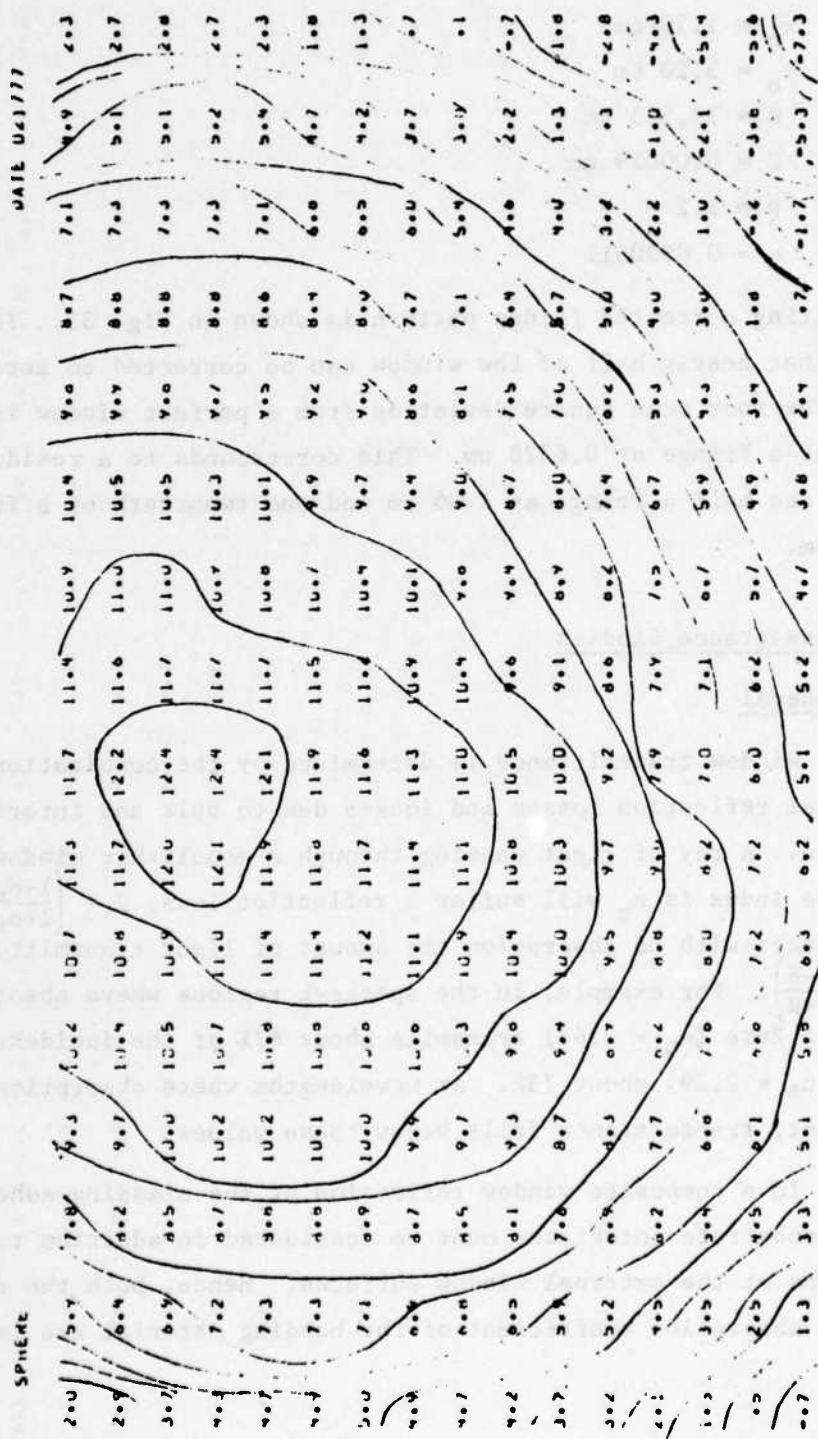


Fig. 32. Fringe matrix of the composite window photographed in Fig. 28.

parameters for the nonlinear optimization. The final optimization yielded the values:

$$\begin{aligned}x_o &= 1.20 \text{ cm} \\y_o &= 3.20 \text{ cm} \\R &= 73,363 \text{ cm} \\C &= 0.00029 \text{ cm} \\\theta &= 1.2 \\\alpha &= 0.000051.\end{aligned}$$

The resulting corrected fringe pattern is shown in Fig. 33. It is evident that nearly half of the window can be corrected to zero fringe order. The root mean square deviation from a perfect window is three-fourths of a fringe at $0.6328 \mu\text{m}$. This corresponds to a residual phase error of one half a fringe at $1.06 \mu\text{m}$ and one twentieth of a fringe at $10.6 \mu\text{m}$.

4.3 Transmittance Studies

4.3.1 General

Window transmittance is determined by the combination of interfacial reflection losses and losses due to bulk and interfacial absorption. A ray of light passing through a monolithic window whose refractive index is n_g will suffer a reflection loss, $R = \left(\frac{1-n_g}{1+n_g}\right)^2$, at each surface; with no absorption the amount of light transmitted will be $T = \frac{1-R}{1+R}$. For example, in the spectral regions where absorption is negligible ZnSe ($n_g = 2.62$) transmits about 67% of the incident light and ZnS ($n_g = 2.29$) about 73%. At wavelengths where absorption is significant, transmittance falls below these values.

In a composite window reflection at the cladding-adhesive and adhesive-substrate interfaces must be considered in addition to reflections at the external window surfaces. Hence, both the refractive index and absorption coefficient of the bonding material are important

SPHERA	DATE 02/1/77																			
-3.1	-1.1	-0.8	-0.6	-0.6	-0.5	-0.1	-0.1	-0.1	-0.4	-0.4	1.3	1.3	1.4	1.3						
.0	-2.4	-0.3	-0.7	-0.4	-0.9	-0.3	-0.3	.1	-0.4	-0.3	.2	.7	1.2	1.4						
.0	.0	-1.0	-0.3	-0.2	-0.7	-0.9	-0.2	-0.2	.2	-0.2	-0.4	.0	.3	1.0						
.0	.0	.1	-1.3	-0.4	-0.1	-0.6	-0.9	-0.1	-0.1	.1	-0.3	-0.3	-0.2	.4						
.0	.0	.0	.0	-0.7	-0.2	-0.1	-0.3	-0.3	-0.3	-0.3	-0.1	-0.3	-0.6	-0.4						
.0	.0	.0	.0	-0.3	-0.0	-0.1	-0.3	-0.4	-0.4	-0.4	-0.3	-0.3	-0.4	-0.6						
.0	.0	.0	.0	.0	-0.2	.0	.1	-0.0	-0.0	-0.4	-0.4	-0.2	-0.3	-0.4						
.0	.0	.0	.0	.0	.0	.0	.2	.2	.4	.3	.1	-0.1	-0.1	-0.3						
.0	.0	.0	.0	.0	.0	.0	.2	.2	.4	.6	.3	.2	.1	-0.0						
.0	.0	.0	.0	.0	.0	.0	.0	.0	.2	.6	.7	.6	.2	.1						
.0	.0	.0	.0	.0	.0	.0	.0	.0	1.1	.4	.7	.8	.6	.4						
.0	.0	.0	.0	.0	.0	.0	.0	.0	.0	2.0	.3	.6	.6	.6						
.0	.0	.0	.0	.0	.0	.0	.0	.0	.0	.0	2.6	.3	.8	.4						
.0	.0	.0	.0	.0	.0	.0	.0	.0	.0	.0	.0	6.4	.3	.7						
-2.1	.0	.0	.0	.0	.0	.0	.0	.0	.0	.0	.0	.0	.3	.5						
1.3	.0	.0	.0	.0	.0	.0	.0	.0	.0	.0	.0	.0	.0	.3						
1.3	1.4	.0	.0	.0	.0	.0	.0	.0	.0	.0	.0	.0	.0	1.2						

Fig. 33. Fringe order matrix of corrected window.

in determining the transmittance of the composite. Figures 34a and b illustrate the transmittance of a 0.032 in. thick (about 810 μm) sample of the glass B used to join composite windows; the short wavelength data were measured on a Cary Model 14 Spectrometer, the long wavelength data on a Digilab Fourier Transform Spectrometer. There is no appreciable absorption from about 0.7 to 10 μm ; what absorption is present between 0.6 to 0.7 μm and 10 to 12 μm in this thick sample will be negligible in the actual bond layers which are less than 10 μm thick. From the magnitude of the transmittance in the absorption free region, about 75%, we estimated that the refractive index of the glass is about 2.20 to 2.25.

4.3.2 Transmittance of Uncoated Composite Windows

The long wavelength transmittance of a composite formed by cladding a 0.060 in. ZnS layer to ZnSe with glass B is illustrated in Fig. 35. Note that since the refractive indices of the ZnS cladding and the glass bonding material are nearly identical, there is negligible reflection loss at the ZnS-glass interface. Analysis of the composite reduces to the case of a layer of ZnS, where thickness is much greater than the wavelength of the incident radiation, on a ZnSe substrate. Calculation shows that there is some reduction in reflection for a layer of lower refractive index in intimate contact with a higher refractive index substrate, although the reduction in reflection is not as great as might be achieved with a thin anti-reflection film of the same material. Indeed, Fig. 35 shows that the transmittance of the composite window is about 75% compared to 67% calculated for the ZnSe window alone. As described below, anti-reflection coatings deposited onto the composite window will further enhance the transmittance. It should be noted here that if the refractive index of the bonding agent were significantly greater (or smaller) than the materials being joined, additional reflection losses would occur and the transmittance of the composite window would be reduced. Figure 35 also shows that the ZnS/ZnSe composite has absorption losses in the

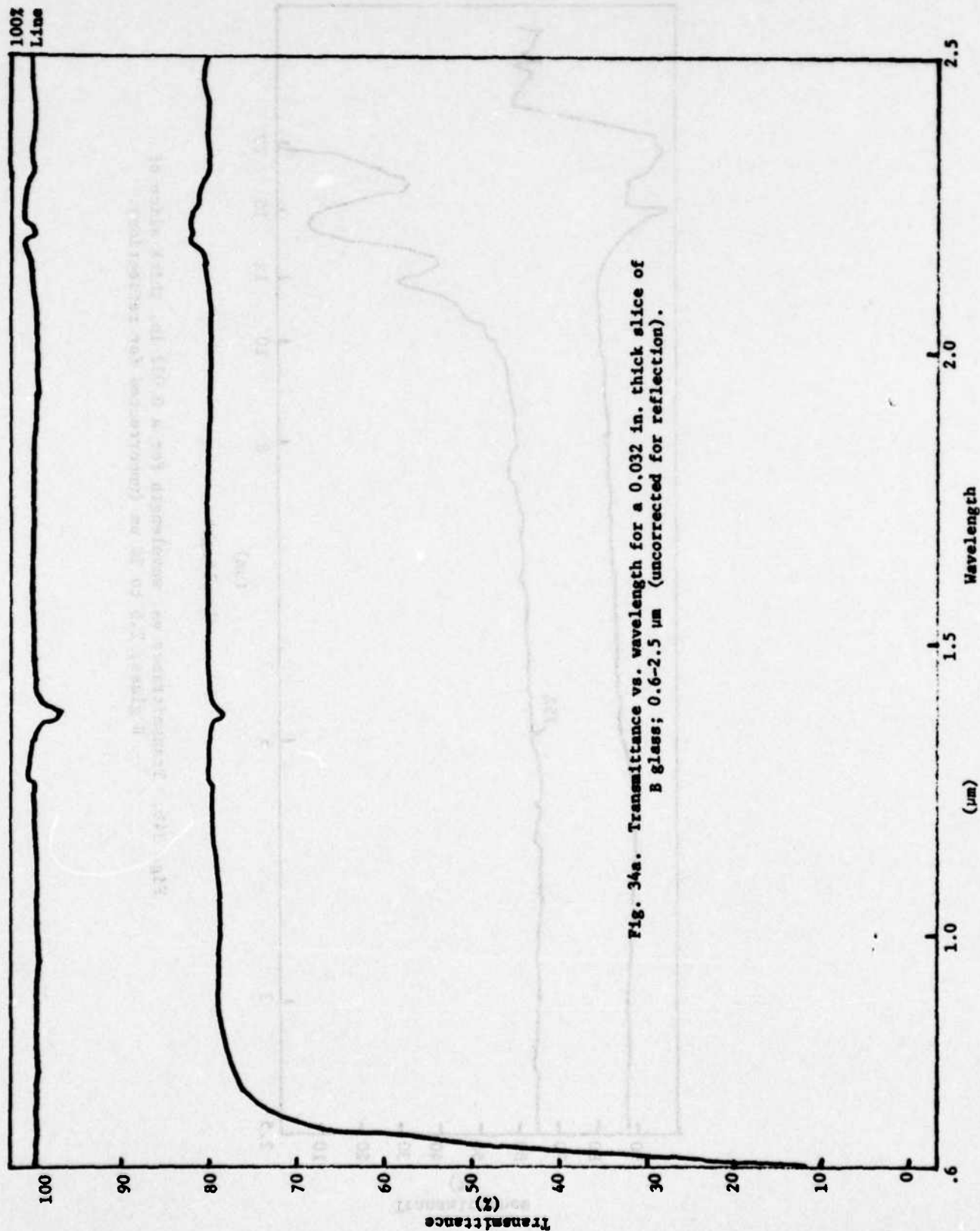


Fig. 34a. Transmittance vs. wavelength for a 0.032 in. thick slice of B glass; 0.6-2.5 μm (uncorrected for reflection).

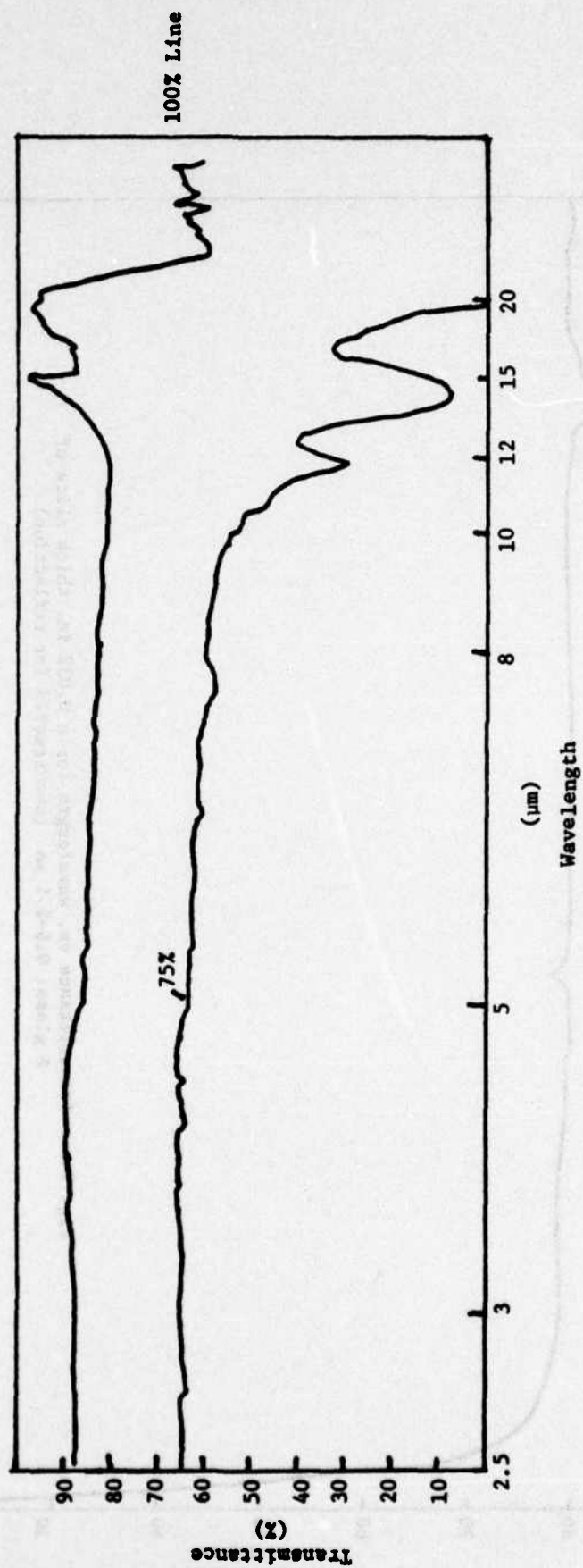


Fig. 34b. Transmittance vs. wavelength for a 0.032 in. thick slice of B glass; 2.5 to 20 μm (uncorrected for reflection).

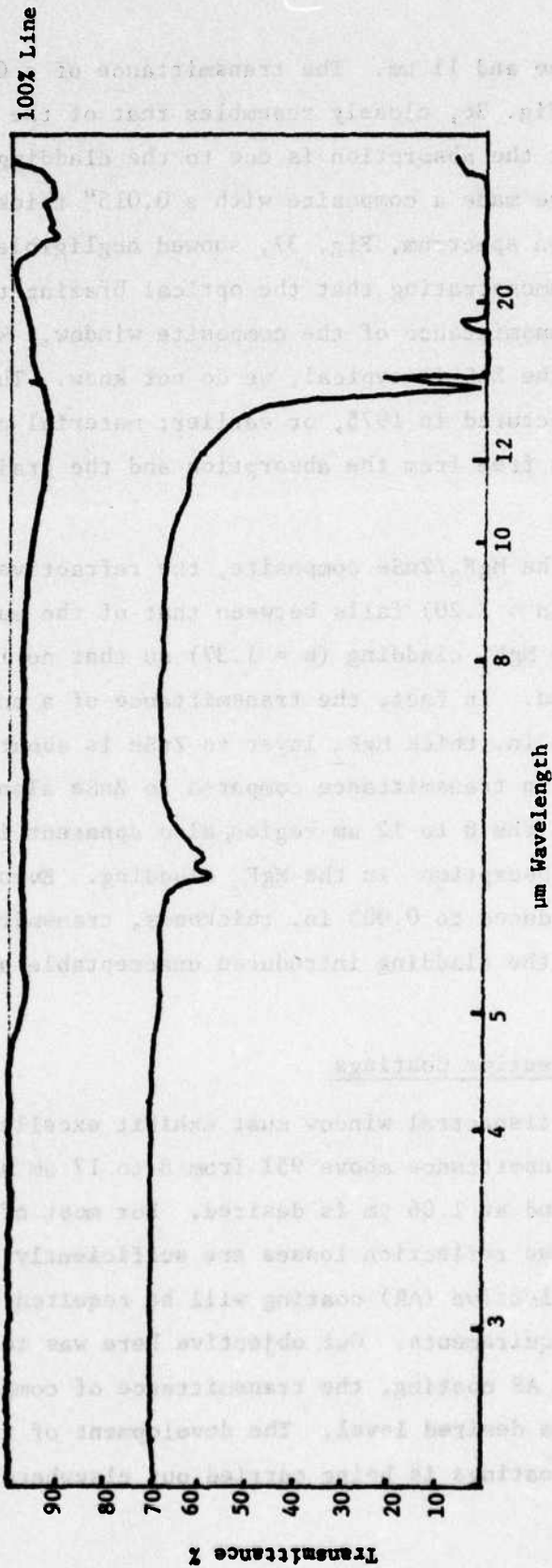


Fig. 35. Transmittance vs. wavelength for 0.060 in. ZnS layer bonded to ZnSe with glass B (No AR coating).

vicinity of 6 μm and 11 μm . The transmittance of a 0.050 in. thick piece of ZnS, Fig. 36, closely resembles that of the ZnS/ZnSe composite indicating that the absorption is due to the cladding, not the substrate. Subsequently, we made a composite with a 0.015" thick ZnS cladding; its transmission spectrum, Fig. 37, showed negligible absorption from 0.6 to 14 μm demonstrating that the optical brazing technique does not degrade the transmittance of the composite window. Whether the absorption in the ZnS is typical, we do not know. The material was probably manufactured in 1975, or earlier; material produced more recently may be free from the absorption and the grain structure noted in Section 3.

For the MgF_2/ZnSe composite, the refractive index of the bonding glass ($n \sim 2.20$) falls between that of the substrate ($n = 2.62$) and that of the MgF_2 cladding ($n = 1.37$) so that no increase in reflection loss is expected. In fact, the transmittance of a composite made by joining a 0.010 in. thick MgF_2 layer to ZnSe is about 77%, Fig. 38, a 10% increase in transmittance compared to ZnSe alone. The decreased transmission in the 8 to 12 μm region, also apparent in Fig. 38, is attributed to absorption in the MgF_2 cladding. Even when the MgF_2 cladding was reduced to 0.003 in. thickness, transmittance measurements indicated that the cladding introduced unacceptable absorption in the 8-12 μm region.

4.3.3 Antireflective Coatings

A multispectral window must exhibit excellent broadband optical properties; transmittance above 95% from 8 to 12 μm and over 60% from 0.5 to 0.9 μm and at 1.06 μm is desired. For most of the candidate composite windows reflection losses are sufficiently great that some type of antireflective (AR) coating will be required to meet the overall transmission requirements. Our objective here was to demonstrate that with a suitable AR coating, the transmittance of composite windows could be raised to the desired level. The development of rain erosion resistant multispectral coatings is being carried out elsewhere.⁴

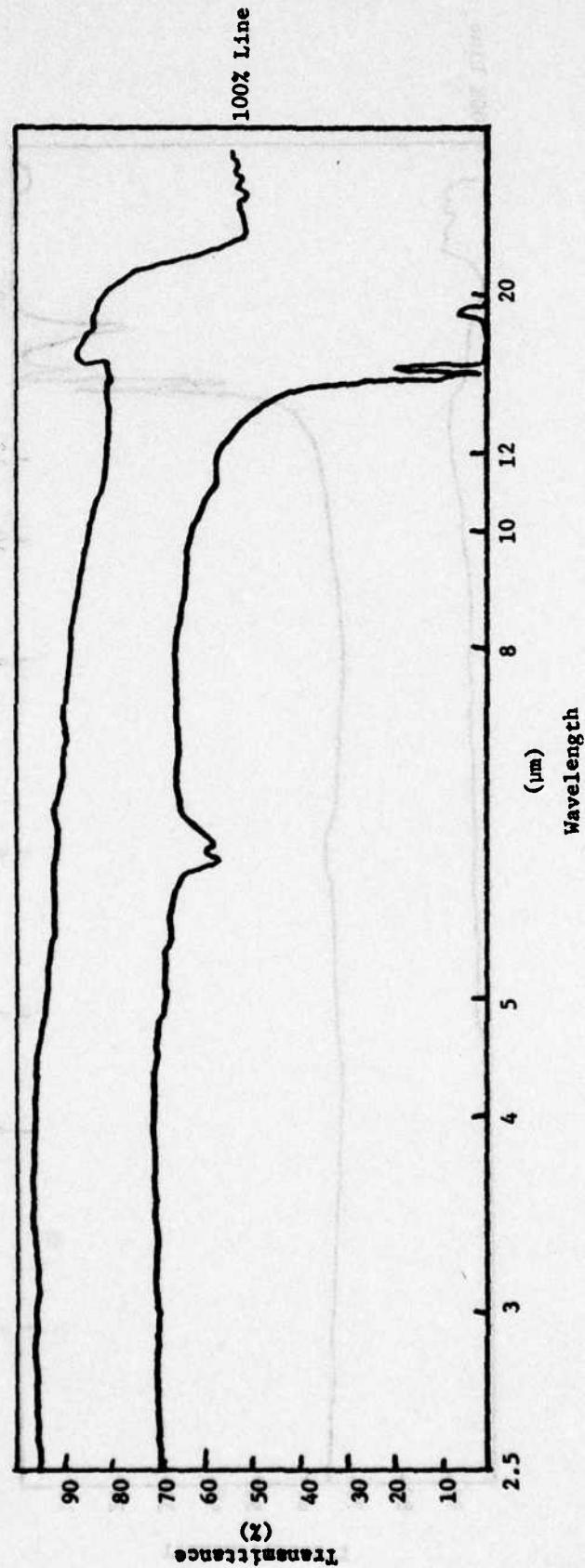


Fig. 36. Transmittance vs. wavelength for a 0.050 in. thick CVD ZnS plate (No AR coating).

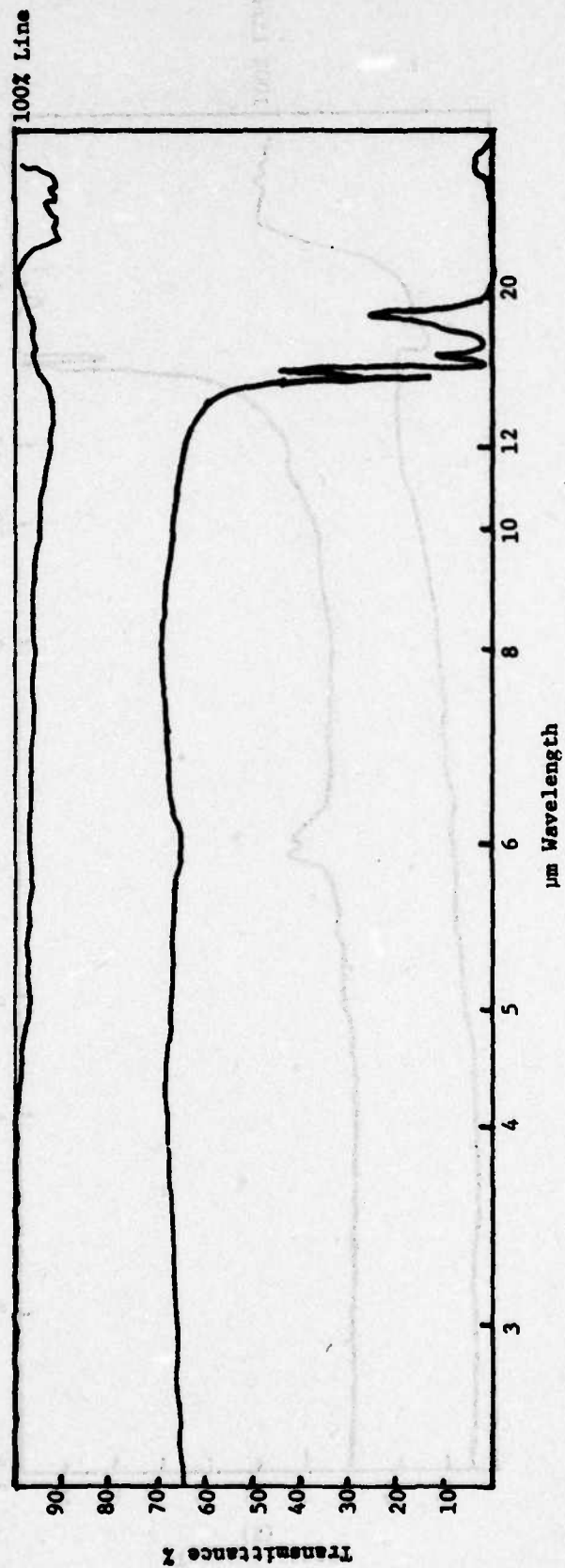


Fig. 37. Transmittance of a ZnS/ZnSe composite formed by bonding a 0.015 in. thick ZnS plate to ZnSe (No AR coating).

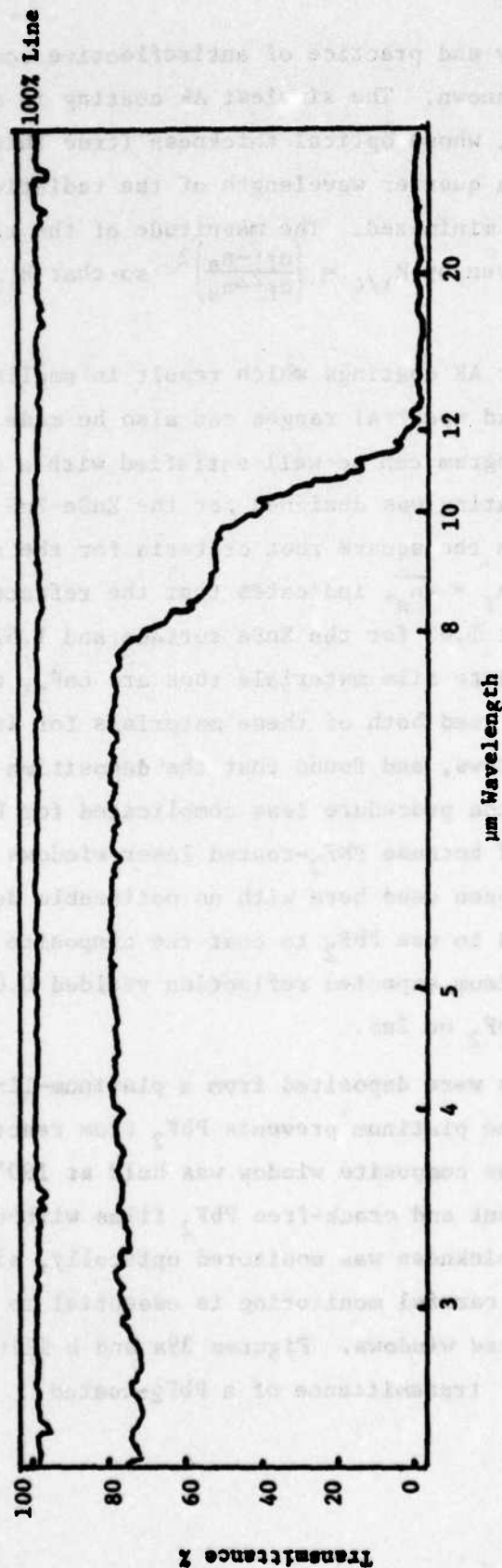


Fig. 38. Transmittance versus wavelength for a MgF₂/ZnSe composite fabricated by joining a 0.010 in. Irtran MgF₂ layer to ZnSe with glass C.

The theory and practice of antireflective coatings for windows and lenses is well known. The simplest AR coating is a single film with refractive index n_f , whose optical thickness (true thickness/refractive index) is equal to a quarter wavelength of the radiation where the reflection is to be minimized. The magnitude of the reflection at the $\lambda/4$ condition is given by $R_{\lambda/4} = \left(\frac{n_f^2 - n_s}{n_f^2 + n_s} \right)^2$ so that $R_{\lambda/4}$ becomes zero when $n_f = (n_s)^{1/2}$.

Multilayer AR coatings which result in smaller values of the reflection over broad spectral ranges can also be made. However, the goals of present program can be well satisfied with a single layer coating. Such a coating was designed for the ZnSe-ZnS composite window. For this combination the square root criteria for the refractive index of the film, i.e., $n_f = \sqrt{n_s}$, indicates that the refractive index of the film should be about 1.62 for the ZnSe surface and 1.51 for the ZnS surface. Two candidate film materials thus are LaF_3 , $n = 1.57$ and PbF_2 , $n = 1.65$. We used both of these materials for initial coating studies on ZnSe windows, and found that the deposition conditions are less stringent and the procedure less complicated for PbF_2 than for LaF_3 . For this reason, and because PbF_2 -coated laser windows over two years old have been used here with no noticeable degradation of the coatings, we decided to use PbF_2 to coat the composite windows. Calculations for the minimum expected reflection yielded 0.04% for PbF_2 on ZnSe and 0.7% for PbF_2 on ZnS.

PbF_2 films were deposited from a platinum-lined tungsten evaporation boat; the platinum prevents PbF_2 from reacting with tungsten. During deposition the composite window was held at 190°C , a temperature found to give adherent and crack-free PbF_2 films without degrading the glass bond. Film thickness was monitored optically, since our previous work indicated that careful monitoring is essential to obtain maximum transmission of coated windows. Figures 39a and b illustrate the short and long wavelength transmittance of a PbF_2 -coated

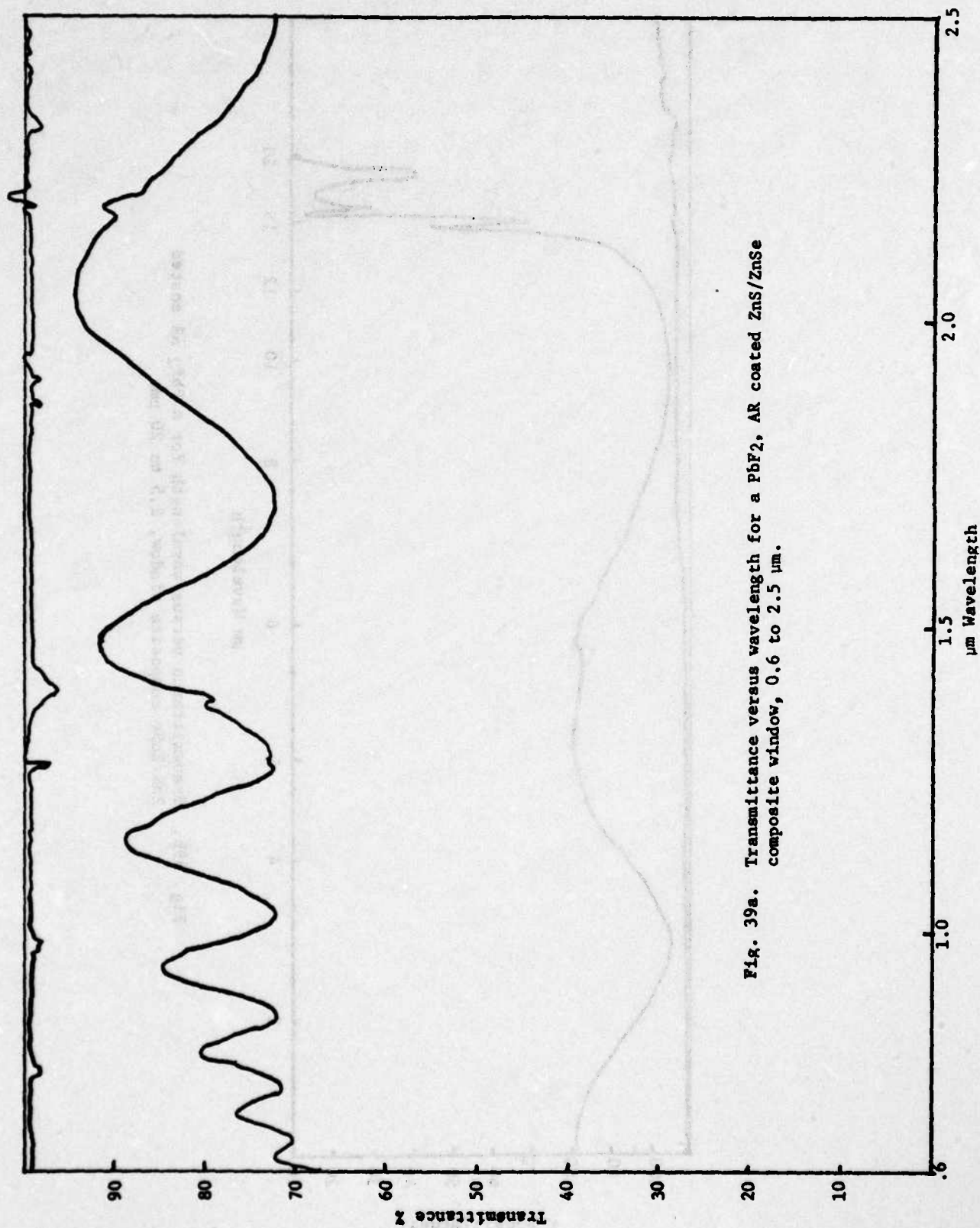


Fig. 39a. Transmittance versus wavelength for a PbF_2 , AR coated ZnS/ZnSe composite window, 0.6 to 2.5 μm .

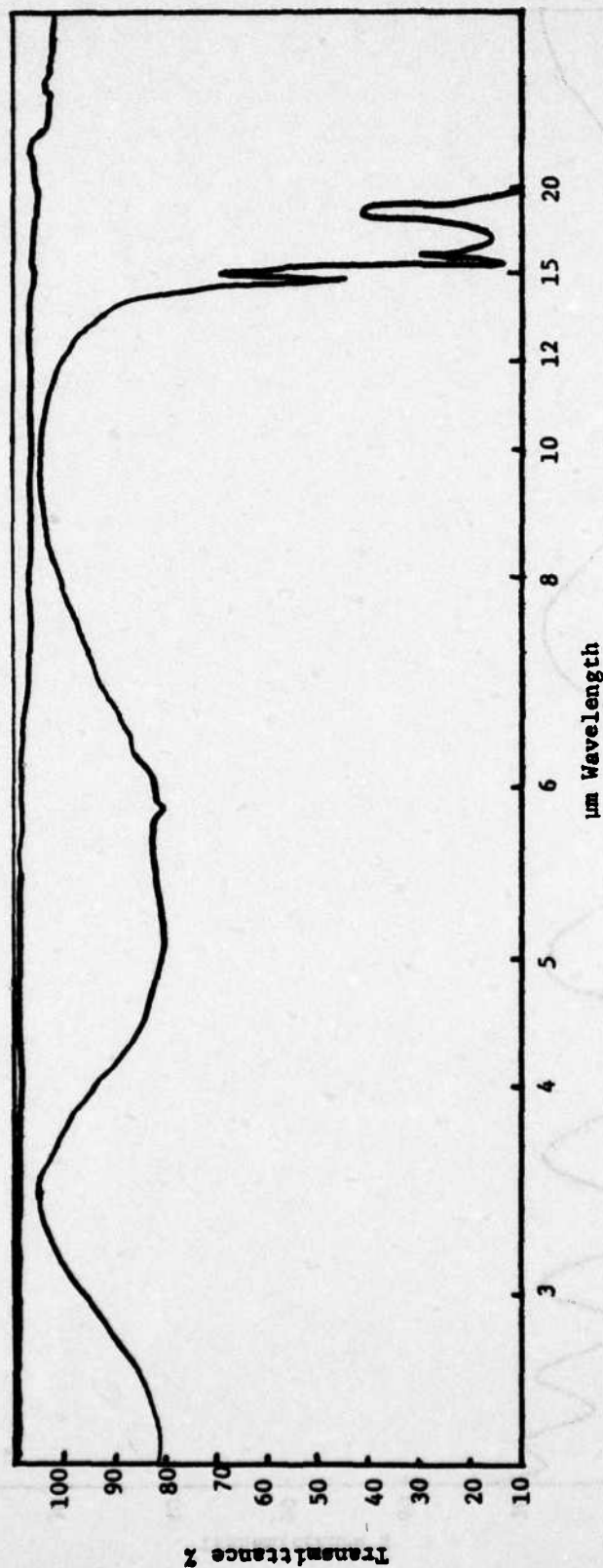


Fig. 39b. Transmittance versus wavelength for a PbF₂ AR coated ZnS/ZnSe composite window, 2.5 to 20 μm.

ZnSe-50% S glass-ZnS composite window. The window was coated on both surfaces with films designed to give peak transmittance at 10 μm . Examination of Fig. 39 shows that the coating process did not introduce any apparent absorption and that the transmittance of the coated ZnSe-ZnS window exceeds the desired levels in the spectral regions of interest.

4.4 Thermophysical Properties

Knowledge of the thermal behavior of window materials and window components is important both for optical design, and for assessing the compatibility of various materials during fabrication and service. The type of calculations that can be performed with such data are diverse. Thus, we have collected from the literature¹⁹ values of thermal expansion, thermal conductivity, and specific heat for the claddings, substrates and glasses used to fabricate the composite windows evaluated during this study. Where such information was scarce or absent, we supplemented the literature data with our own measurements.

In the case of thermal expansion, data were gathered with a horizontal quartz tube dilatometer. The change in specimen length sensed by a strain gage transducer was recorded along with specimen temperature on a two coordinate recorder. The cooling and heating rates were automatically programmed and all measurements were made in air. Thermal conductivity was determined by the stationary heat flow method. The 0.5 x 0.5 in. cylindrical samples were ultrasonically soldered to the heater and heat sink of the calorimeter which has been described in detail elsewhere.^{21,22} Measurement accuracy is estimated at $\pm 2\%$. Typical data for two bonding glasses measured over the temperature interval 190 to 380K appear in Fig. 40.

The data for all materials are compiled in Table 5. The high thermal expansion coefficients of the glass bonding agents are notable, but typical for chalcogenides of this type. Apparently, the resiliency

Curve 688433-A

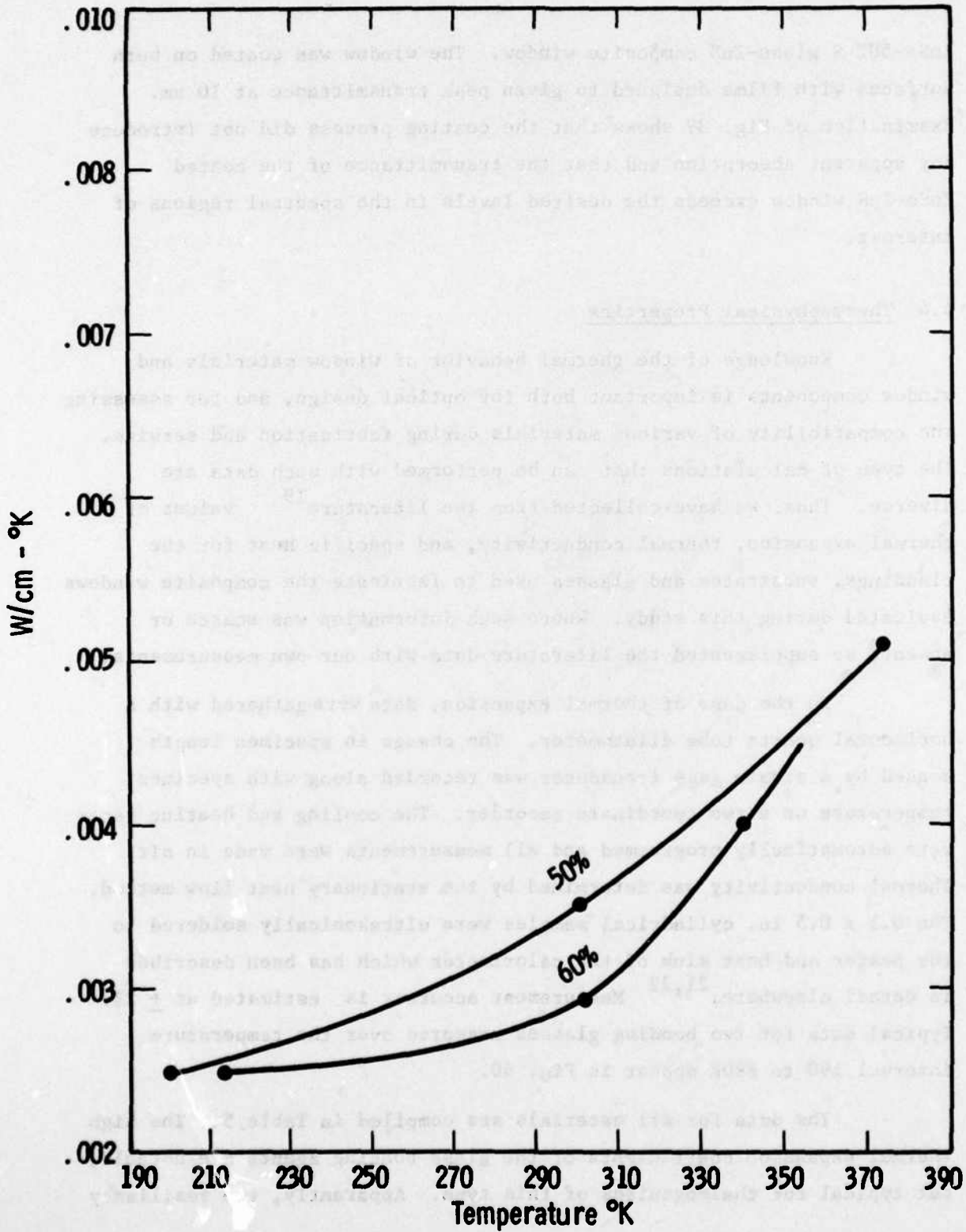


Fig. 40. Thermal conductivity of 50 and 60% S glass bonding agents from 190 to 380K.

TABLE 5

Thermophysical Properties of Substrates, Claddings and Glasses
Used to Fabricate Composite Multispectral Windows

	Thermal Expansion $\alpha \times 10^{-6}/^{\circ}\text{K}$	Thermal Conductivity $\text{K} \times 10^{-4} \text{ cal/cm, sec, } ^{\circ}\text{K}$	Specific Heat $\text{J/cm}^3, ^{\circ}\text{K}$
ZnSe	7.5-8.2	310	1.88
KCl	36	167	1.39
NaCl	23-40	157	1.96
ZnS	6.6-7.5	370	1.99
MgF ₂	10.6-12	350	2.93
CaF ₂	19.7-24	190	2.71
50% S glass	49	8	
60% S glass	49	7	

of the glasses, coupled with the relatively large expansion coefficient and good wetting properties is responsible for the remarkable ability of these materials to join materials with considerably different thermal expansion coefficients.²²

4.5 Mechanical Properties

4.5.1 Hardness and Strength of Window Components

Collected in Table 6 are typical values of the hardness and strength of the various window components we evaluated. The data were taken from the literature¹⁹ or measured during the program. Generally the rain erosion test data (see below) correlate well with the hardnesses of the various materials: MgF_2 and ZnS are most erosion resistant and ZnSe the least.

4.5.2 Bond Strength

A crude measure of the strength of the glass bond joining the window composites was made by tensile testing a pair of 0.5 x 0.5 in. ZnS/ZnSe specimens. A load was applied normal to the joined surfaces after the composite specimens had been cemented to steel grips with 3M AF42 adhesive. The tests were made on a Baldwin Universal Testing Machine. The breaking strength of the 50% S glass joint was 1688 lb/in²; that of a specimen bonded with the 60% S glass was 1704 lb/in². While these data cannot be compared directly with the known strengths of ZnS or ZnSe normally measured in flexure tests, the fracture surfaces of the test pieces clearly indicate that it is the ZnSe, not the glass which failed, e.g., Fig. 41. The crack path cut transgranularly through ZnSe (light) then through the glass layer into the ZnS. The dark areas are places where loose material spalled after test. The tenacity of the bond in this static test is evident.

4.5.3 Rain Erosion Testing

Tensile tests give only a partial indication of how a given adhesive will perform in service. This is because the loading of a

TABLE 6

Typical Mechanical Properties of Cladding, Substrates and Glasses
Used to Fabricate Composite Windows

	Microhardness Knoop (kg/mm^2)	Tensile Strength KSI
ZnSe	100-150	4-8.5
KCl	11-14	.8-7.2
NaCl	22-44	3.5-5.7
ZnS	225-250	16
MgF ₂	576	21
CaF ₂	200	2-7
50% S glass	18	
60% S glass	41	

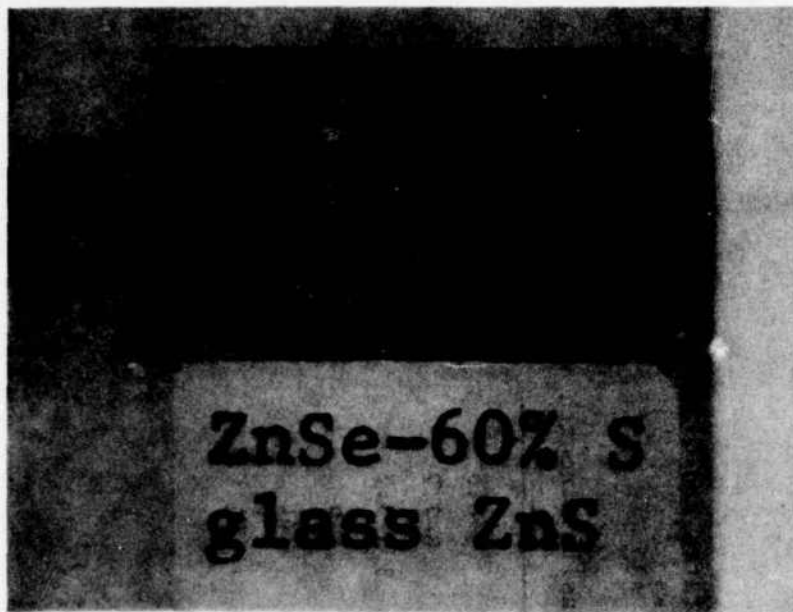


Fig. 41. Fracture surface of ZnS/ZnSe composite tested to failure in tension. The crack path passed primarily through the ZnSe substrate (light). The dark areas are material that spalled after testing.

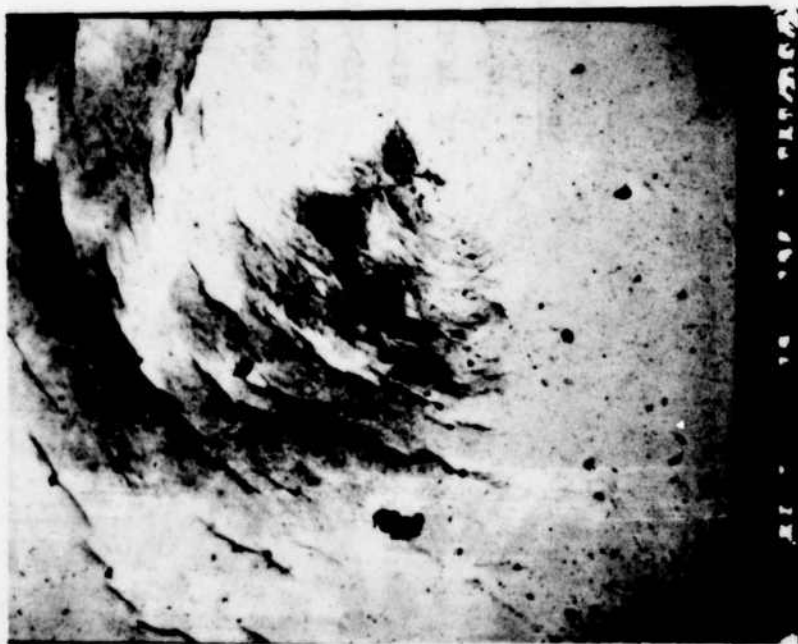


Fig. 42. Ring cracks formed in the ZnS cladding of a ZnS/ZnSe composite rain erosion specimen after exposure to the simulated rain field.

material during rain erosion is dynamic in nature, involving elements of impact and cyclic stressing. For this reason more than twenty (20) composites fabricated by us have been evaluated for rain erosion resistance in the AFML centrifugal test facility at Wright Field (see e.g. Ref. 6). The cladding material and thickness, the substrate material, and the adhesive were varied to assess the relative merits of various combinations. The test conditions were one in/hr simulated rainfall at 470 mph specimen velocity. Following periodic exposure, each specimen was examined in the optical microscope, and its transmittance was measured over the 2.5 to 25 μ m spectral range.²³

The erosion data for some representative specimens are compiled in Table 7; for completeness some data from earlier tests (marked 0) are included. The most salient result of the experiment was that the glass bonded CVD ZnS/CVD composite showed essentially the same erosion resistance as monolithic CVD ZnS.²³ The ring cracks formed on the composite after prolonged exposure, Fig. 42, are quite similar to those on ZnS.¹⁴⁻¹⁶ This is in contrast to Irtran ZnS/ZnSe windows which had inferior erosion resistance in earlier trials. The erosion tests also demonstrated two other important features of optically-brazed composites: (1) the glass bond is durable; it does not delaminate during dynamic rain impact and (2) cracking is primarily confined to the ZnS cladding unless the cladding thickness falls below about 0.020 inch. (This suggests that the damaged cladding could be periodically removed and replaced with undamaged material at considerably less cost than replacing the whole window.) Clearly, the data are yet insufficient to determine the optimum ZnS cladding thickness, and this should be a subject of future work.

The MgF_2/ZnS test data mirror the ZnS/ZnSe data with respect to the durability of thicker layers. Single crystal and Irtran MgF_2 are both relatively erosion resistant as might be predicted from their hardness. However, single crystal MgF_2 shows a tendency to delaminate,

TABLE 7

Rain Erosion Test Data for Representative Composites
470 mph, /in/hr rainfall

WEL. #	AGE. #	Substrate	Bonding Agent	Cladding	Cladding Thickness	Exposure - Angle	Results
O 22	3672	ZnSe	60X S glass	INTRAM MgF ₂	30 mil	10 min 78° impact	MgF ₂ essentially undamaged. Specimen broken. Small transmission loss measured probably due to large cracks.
O 23	3673	ZnSe	60X S glass	Single MgF ₂	30 mil	10 min 78° impact	MgF ₂ layer removed after between 5 and 10 min exposure. Single drop imprint visible in exposed adhesive.
O 25	3674	ZnSe	60X S glass	INTRAM MgF ₂	25 mil	10 min 78° impact	MgF ₂ essentially undamaged. Specimen broken. Small transmission loss measured.
E-6	7346	ZnSe	60X S glass	INTRAM MgF ₂	10 mil	20 min 90° impact	Network of cracks in MgF ₂ . Considerable damage initiated at interface and propagated into ZnSe.
E-7	7347	ZnSe	60X S glass	Single MgF ₂	3 mil	20 min 90° impact	MgF ₂ layer removed. Considerable cracking and pitting in glass interlayer and ZnSe.
O 27	5676	ZnSe	Loctite 307	Single MgF ₂	30 mil	5 min 78° impact	MgF ₂ layer cracked. Some cracks in ZnSe substrate. Some delamination.
O 26	5875	ZnSe	60X S glass	CVD ZnS	30 mil	10 min 78° impact	Ring cracking in ZnS. Specimen broken. Transmission at 2.5 μ m dropped from 73% to 69% and transmission at 10 μ m dropped from 73% to 72% after 5 min exposure.
E-2	7050	ZnSe	50X S glass	CVD Yellow ZnS	60 mil	20 min 78° impact	Ring cracking in ZnS. Cladding broken. Transmission at 2.5 μ m dropped from 68% to 63% and transmission at 10 μ m dropped from 73% to 72%.
E-3	7051	ZnSe	50X S glass	CVD Brown ZnS	60 mil	20 min 78° impact	Ring cracking in ZnS. Transmission at 2.5 μ m dropped from 69% to 67% and transmission at 10 μ m dropped from 73% to 72-1/2%.
E-8	7534	ZnSe	50X S glass	CVD ZnS	60 mil	20 min 90° impact	Sample cracked. Ring cracking in ZnS layer. Damage confined to ZnS layer except for a few large cracks.
E-9	7535	ZnSe	50X S glass	CVD ZnS	15 mil	20 min 90° impact	Ring cracking in ZnS layer. Some cracking in ZnSe substrate.
E-10	7640	ZnSe		2114 Epoxy	3 mil	10 min 90° impact	Sample completely destroyed.
E-11	7641	Marshaw	2114 Epoxy	INTRAM CaF ₂	40 mil	10 min 90° impact	Sample completely destroyed.
E-12		ZnSe	50X S glass	CVD ZnS	60 mil	20 min 90° impact	Ring cracking in ZnS layer.
E-14		ZnSe	50X S glass	CVD ZnS	60 mil	20 min 90° impact	Ring cracking in ZnS layer.
E-15		ZnSe	50X S glass	CVD ZnS	10 mil	Not Tested	AR coated.
E-16		ZnSe	50X S glass	CVD ZnS	76 mil	Not Tested	

leading to substrate cracking. Irtran MgF_2 provides good protection until the cladding thickness reaches the 0.010 to 0.015 in. range, then crack propagation into the substrate becomes very evident. This is significant because the transmittance of Irtran MgF_2 is sufficiently low in the 8 to 12 μm region that rather thin claddings would be required to meet optical requirements with present quality material (Section 4.3).

Specimens bonded with the organic adhesives generally delaminated. Composites based on salt substrates were completely destroyed.

SECTION V

CONCLUSIONS

The primary objective of this study, to develop a rain erosion resistant composite multispectral window, has been successfully accomplished. ZnS clad to ZnSe by a Westinghouse-developed technique called optical brazing meets both the optical and mechanical requirements for airborne common aperture systems. Both 2 x 2 in. and 4 x 6 in. ZnS/ZnSe windows were fabricated with no major modifications to the joining process indicating that the method should be scalable to the larger window sizes envisaged for systems applications. At present the most difficult step to scale-up appears to be the uniform polishing of the cladding but even this appears feasible.

Computer analysis of the interferograms taken from the ZnS cladding, ZnSe substrate and assembled composite window indicates that the major sources of optical path differences are the window components themselves. The transparent glass used to bond the polished pieces introduces no significant degradation in the optical homogeneity of the window. Moreover, the optical path differences that are present can be minimized by suitable corrections during the final polishing of the assembled composite.

The transmittance of the ZnS/ZnSe windows is sufficiently good that with a suitable antireflective coating, e.g., LaF_3 or PbF_2 , the windows meet or exceed the minimum system requirements. The results of rain erosion tests on optically-brazed composites verify that the ZnS/ZnSe windows are as erosion resistant and monolithic as ZnS. Fracture when it occurs during rain impingement can be confined to the cladding layer when the ZnS is thicker than about 0.020 in. In practice, the damaged cladding could be replaced periodically allowing the window to be maintained at relatively low cost.

Optical brazing is versatile and other cladding-substrate combinations have been joined. For example, MgF_2/ZnSe windows up to 2 x 2 in. size were readily fabricated. The low long wavelength transmittance of present hot-pressed MgF_2 limits the utility of this erosion resistant composite window.

A number of organic optical cements also appear promising for sandwich window construction. Their primary limitations are the difficulty of controlling cement thickness, uniformity and homogeneity during joining and the tendency of the bonds to delaminate during rain erosion testing.

REFERENCES

1. A. R. Hilton, J. Electronic Mat. 2, 211 (1973).
2. J. Pappis, R. Donadio, and A. Swanson, Technical Report AFML-TR-75-142, Air Force Materials Laboratory (1975).
3. J. Pappis, B. A. di Benedetto, Technical Report AFML-TR-75-27, Air Force Materials Laboratory (1975).
4. D. Fischer, AFML, Communication 1976.
5. W. E. Kramer and R. H. Hopkins, unpublished results (1974).
6. G. F. Schmidt, "Rain Droplet Erosion Mechanisms in Transparent Plastic Materials," presented at Mechanical Failures Prevention Group Meeting, Boulder, Colorado (1973).
7. W. F. Adler, "Characterization of Transparent Materials for Erosion Resistance," AFML Reports on Contract F33615-73-C-5057 (1973).
8. G. Hoff and H. Rieger in Proceedings of the 11th Symposium on Electromagnetic Windows, ed. N. E. Paulos and J. D. Walton, Jr. Georgia Institute of Technology, p. 93 (1972).
9. G. S. Springer et al., "Analysis of Rain Erosion of Coated Materials," J. Comp. Mat. 8, 229 (1974).
10. C. S. Springer and C. B. Baxi, "A Model for Rain Erosion of Homogeneous Material," ASTM Symposium on Erosion, Wear, and Interfaces with Corrosion, June 1973.
11. Y. C. Huang, "Numerical Studies of Unsteady Two-Dimensional, Liquid Impact Phenomena," Ph.D. Dissertation, University of Michigan (1971).
12. M. Rosenblatt et al., Interim Report on "Influence of Interactive Stress States on Erosion Mechanisms of Infrared-Transparent Materials," AFML Contract F33615-75-C-5081 (1975).

13. W. B. Hillig, "Impact Studies of Polymeric Matrices," Naval Air Systems Command, Contract N00019-72-C-0218 (1973).
14. W. F. Adler, "Particulate Erosion of Glass Surfaces at Subsonic Velocities," J. Noncrystalline Solids 19, 335 (1975).
15. W. F. Adler, "Exploratory Development of Supersonic Rain, Sand, and ICL Erosion Resistant Materials," Air Force Materials Laboratory, Quarterly Report No. 1, Contract F33615-76-C-5125, June 1976.
16. W. F. Adler, Ibid., Quarterly Report No. 2, September 1976.
17. S. S. Flaschen, A. D. Pearson, and W. A. Northover, "Low-Melting Inorganic Glasses with High Melt Fluidities Below 400°C," J. Amer. Cer. Soc. 42, 450 (1959).
18. M. D. Williams and E. C. Foust, "Spectral Transmittance Characteristics of Adhesives from 0.2 to 15 Microns," NWC T P5583, Naval Weapons Center (March 1974).
19. S. K. Dickenson, Technical Report AFCRL-TR-75-03018, June (1975); J. C. Worst and T. P. Graham, Technical Report AFML-TR-75-28, April (1975); W. F. Adler and S. V. Hooker, Technical Report AFML-TR-76-16, March (1976); C. S. Sahagian and C. A. Pithor, Technical Report AFCRL-72-0170, March (1972).
20. D. H. Damon, J. Appl. Phys. 37, 3181 (1966).
21. R. H. Hopkins et al., JAP 42, 272 (1971).
22. S. S. Flaschen et al., J. Amer. Cer. Soc. 43, 274 (1960).
23. T. L. Peterson, Air Force Materials Laboratory, Communication (1976-77).

